NASA TECHNICAL NOTE

STARTING PHENOMENA FOR HYPERSONIC INLETS WITH THICK TURBULENT BOUNDARY LAYERS AT MACH 6

by Theodore J. Goldberg and Jerry N. Hefner

Langley Research Center
Hampton, Va. 23365

NATIONAL AERONAUTICS AND SPACE ADMINISTRATION • WASHINGTON, D. C. • AUGUST 1971

1. Report No.	2. Government Accession No.	3. Recipient's Catalog No.
NASA TN D-6280		

4. Title and Subtitle

STARTING PHENOMENA FOR HYPERSONIC INLETS WITH THICK TURBULENT BOUNDARY LAYERS AT MACH 6

5. Report Date: August 1971

6. Performing Organization Code:

7. Author(s)

Theodore J. Goldberg and Jerry N. Hefner

8. Performing Organization Report No.: L-7665

9. Performing Organization Name and Address

NASA Langley Research Center
Hampton, Va. 23365

10. Work Unit No.: 764-75-01-05

11. Contract or Grant No.:

12. Sponsoring Agency Name and Address

National Aeronautics and Space Administration
Washington, D.C. 20546

13. Type of Report and Period Covered: Technical Note

14. Sponsoring Agency Code:

15. Supplementary Notes

Appendix – Description and Calibration of the Langley 20-Inch Mach 6 Tunnel by James C. Emery.

16. Abstract

The effects of cowl length, cowl bluntness, cowl angle of attack, boundary-layer thickness, free-stream Reynolds number, and wall temperature on the starting phenomena of two-dimensional hypersonic inlets with turbulent intake boundary layers were experimentally investigated at a free-stream Mach number of 6. The inlet total-pressure recovery (including both shock and viscous losses) governs starting in contrast to only the normal-shock pressure recovery usually considered. The total-pressure recovery required for starting is predicted reasonably well by a one-dimensional analysis.

17. Key Words (Suggested by Author(s))

Inlets
Hypersonic
Inlet starting
Pressure recovery
Turbulent boundary layers
Inlet contraction ratio

18. Distribution Statement

Unclassified – Unlimited

19. Security Classif. (of this report)	20. Security Classif. (of this page)	21. No. of Pages	22. Price*
Unclassified	Unclassified	55	$3.00

*For sale by the National Technical Information Service, Springfield, Virginia 22151

STARTING PHENOMENA FOR HYPERSONIC INLETS WITH THICK TURBULENT BOUNDARY LAYERS AT MACH 6

By Theodore J. Goldberg and Jerry N. Hefner
Langley Research Center

SUMMARY

The effects of cowl bluntness, cowl length, cowl angle of attack, boundary-layer thickness, free-stream Reynolds number, and wall temperature on the starting phenomena of two-dimensional hypersonic inlets with relatively thick turbulent intake boundary layers were investigated at a free-stream Mach number of 6. The inlet total-pressure recovery (including both shock and viscous losses) is the governing factor determining the starting of these inlets; this is in contrast to the generally accepted criterion of considering contraction ratio based only on normal-shock pressure recovery which is applicable to inlets with relatively thin boundary layers.

Although boundary-layer separation in the vicinity of the cowl lip station does not appear to directly govern starting by adversely affecting contraction ratio, it does significantly affect the inlet pressure recovery by increasing the viscous losses through mixing. The geometric and aerodynamic parameters investigated also affect starting by their effect on the pressure recovery.

The total-pressure recovery required for starting these inlets can be predicted reasonably well by a one-dimensional analysis; however, at present there is no accurate means of predicting the total-pressure recovery, accounting for separation and viscous losses as well as internal shock losses, for a given configuration. Basic data is provided which can be used to verify future empirical or theoretical methods to predict inlet pressure recovery and, thus, starting.

INTRODUCTION

For current supersonic inlets with intake heights significantly larger than the boundary-layer thickness, starting (establishment of supersonic flow in the internal passage of the inlet) has been adequately predicted. However, starting phenomena are not fully understood for envisioned hypersonic inlets where the boundary layer comprises a significant portion of the intake flow. This has been demonstrated in the Hypersonic Research Engine (HRE) Project where it was difficult to obtain an inlet start during wind-tunnel tests of an early design inlet model at the design conditions. (See ref. 1.) The

usual analytical methods for the prediction of starting current supersonic inlets are of little value since the complex flow field caused by shock—boundary-layer interactions together with associated separation and mixing within a confined boundary invalidates the initial assumptions usually made for a predominantly inviscid flow. In addition, little data are available as a basis for useful design criteria. Therefore, to gain a better understanding of the starting phenomena and to provide data for future theoretical prediction methods, the present investigation was undertaken. The quantitative effects of geometric and aerodynamic parameters on the starting of a two-dimensional hypersonic inlet with thick turbulent boundary layers relative to the intake height were investigated. A simplified model composed of flat plate elements was tested in order to gain an understanding of the flow which would be applicable to realistic hypersonic inlets. The variables investigated at a free-stream Mach number of 6 were cowl bluntness, cowl length, cowl angle of attack, boundary-layer thickness, free-stream Reynolds number, and model wall temperature.

This report includes an appendix by James C. Emery, of the Langley Research Center, which presents a description and Mach number calibration of the Langley 20-inch Mach 6 tunnel.

SYMBOLS

A	area
A*	area at throat
h	height between centerbody plate and cowl plate
l	length
M	Mach number
$\overline{M}$	mass-weighted Mach number, $\dfrac{\int_0^h M\rho u\, dz}{\int_0^h \rho u\, dz}$
p	pressure
p'	pitot pressure

$\overline{p}$ mass-weighted total pressure, $\dfrac{\int_0^h p_t \rho u \, dz}{\int_0^h \rho u \, dz}$

r leading-edge radius

R unit Reynolds number

s longitudinal distance measured from leading edge of centerbody plate

T temperature

u velocity

x longitudinal distance from cowl lip station (positive in downstream direction)

y spanwise distance along centerbody plate measured from center line

Y semispan of centerbody plate

z vertical distance from centerbody plate

α angle of attack

δ boundary-layer thickness, value of z at which $u = 0.995u_e$

δ^* boundary-layer displacement thickness, $\int_0^\delta \left(1 - \frac{\rho u}{\rho_e u_e}\right) dz$

θ boundary-layer momentum thickness, $\int_0^\delta \frac{\rho u}{\rho_e u_e}\left(1 - \frac{u}{u_e}\right) dz$

ρ density

Subscripts:

c cowl

e conditions at edge of boundary layer

l	local
t	total or stagnation
w	wall
1	conditions at cowl lip station
2	conditions at cowl exit station
∞	free stream

APPARATUS AND METHODS

Model

A drawing of the two-dimensional inlet model is shown in figure 1 and a photograph in figure 2. This simplified inlet model consisted essentially of two flat plates having 30.48-cm spans, mounted between end plates. The upper flat plate, which simulated a cowl, varied in length, leading-edge radius, and angle of attack. Cowl lengths of 5.08, 10.16, and 15.24 cm were tested with leading-edge radii of 0.0025, 0.0762, and 0.1524 cm at angles of attack from 0° to 6° in 2° increments; cowl lengths of 30.48 and 45.72 cm were tested with a leading-edge radius of 0.0762 cm at 2° angle of attack. The lower flat plate, which simulated an inlet centerbody, had a sharp leading edge (0.0025 cm) and was alined parallel to the free-stream flow. The inlet was mounted in the tunnel with the centerbody plate either in the free stream at 6.35 cm below the center line of the test section (fig. 1(a)) or flush with the lower wall of the test section (fig. 1(b)). With the centerbody plate in the free stream, the cowl lip was 58.42 cm downstream of centerbody leading edge. The sidewalls of the inlet contained optical quartz windows (17.75 by 8.88 cm) to obtain schlieren photographs of the flow ahead of, and within, the inlet passage when the model was mounted in the free stream. Rectangular flaps, hinged to the trailing edge of the cowl plate and operated by a pneumatic actuator, were used to choke the inlet passage when desired. The flaps were 0.476 cm thick with a span of 10.16 cm and with varying chord lengths to permit closing off approximately 70 percent of the exit flow area. When the exit flow area was completely open, the trailing edges of the flaps were always above the lower surface of the cowl plate.

Wind Tunnel

This investigation was conducted in the Langley 20-inch Mach 6 tunnel. A detailed description along with the Mach number calibration of the tunnel is presented in the appendix.

Tests

The experimental investigation was conducted at a free-stream Mach number of 6 primarily at a free-stream Reynolds number of 2.06×10^7 per meter (stagnation pressure of 2.86 MN/m^2 and stagnation temperature of 506 K). This test condition resulted in turbulent boundary-layer thicknesses of 1.0 cm with the inlet centerbody in the free stream and 5.1 cm with the inlet centerbody flush with the tunnel wall. Limited tests were also made at Reynolds numbers from 1.08×10^7 to 2.75×10^7 per meter. Most of the data were obtained with the model near adiabatic wall temperature $\left(T_w/T_{t,\infty} = 0.89\right)$ with some additional tests at lower wall temperatures. The free-stream Mach number for these tests varied from 5.95 to 6.04; however, the variation during any one test was ±0.02.

Procedures and Instrumentation

Test procedure.- An investigation of inlet starting requires close control of the boundary layer at the time data are taken. Since boundary layer is influenced by variations in wall temperature, it is necessary to minimize temperature variations during a test run as well as from one run to another. A procedure was devised whereby the desired and repeatable test conditions would be obtained throughout this investigation. With the model wall temperature set approximately at the desired level, either by a preheat flow through the tunnel or by prior cooling with dry ice, the tunnel flow was established. The mechanical flaps at the cowl trailing edge were closed and reopened when the wall temperature was at the desired level. Data and schlieren photographs of selected configurations were obtained before and after the flaps were closed and reopened.

Determination of inlet starting.- Started and unstarted conditions, as well as the presence of separation, were determined from static-pressure distributions along the longitudinal center line of the centerbody and cowl plate and from schlieren photographs. The inlet was considered to be started when the shock from the cowl leading edge was inside the passage and no rapid increase in the static pressure was measured upstream of the cowl leading-edge station. See figure 3 for examples of schlieren photographs and pressure distributions for both started and unstarted configurations.

Instrumentation.- Static-pressure distributions were measured along the longitudinal center line of the centerbody plate and cowl plates. In addition, spanwise static pressures were measured on the centerbody plate. (See fig. 1(a) for orifice locations.) Essentially two-dimensional flow for a span of ±12.7 cm from the center line was found to exist for all configurations tested. Total pressures were determined at the cowl exit station from pitot rake measurements (pitot rake details are presented in fig. 1(c)) and by assuming a straight-line variation of the static pressures between the centerbody plate and the cowl; total pressures at the cowl lip station were calculated from measurements from a pitot rake and a static-pressure orifice on the centerbody plate without the cowl in place. Using

these total-pressure profiles at the cowl lip station and at the exit station, mass-weighted Mach numbers and pressure recoveries were calculated for the various test conditions. The free-stream Mach number was obtained for each test point by measuring the pitot pressure and the stagnation pressure. Iron-constantan thermocouples were used to obtain tunnel stagnation temperature and model wall temperatures.

The static-pressure orifices and pitot probes were connected to a pressure switching device which directed the pressures to multirange capacitance-type pressure transducers. Each pressure was monitored by automatic range selectors which chose the closest of seven discreet ranges each having an equal full-scale output over the pressure range of 0 to 0.133 MN/m^2. Higher readings for the pitot probes were measured with 0 to 0.172 MN/m^2 or 0 to 0.345 MN/m^2 transducers which were teed to the lower multirange transducers. Tunnel stagnation pressures were measured with 0 to 0.69, 0 to 2.07, and 0 to 3.45 MN/m^2 transducers. All pressure and temperature data of this investigation were recorded on magnetic tape and processed by an electronic data processing system; the data could also be monitored visually.

RESULTS AND DISCUSSION

Boundary-Layer Characteristics

The type and relative thickness of the boundary layer entering the inlet is extremely important in inlet technology, and there is a paucity of results where thick boundary layers occur at hypersonic Mach numbers; therefore, the turbulent boundary-layer characteristics (as previously defined in the Symbols) on the inlet centerbody at the cowl lip station are presented in figures 4 and 5. Boundary-layer profiles obtained from pitot- and surface-static-pressure measurements, with a modified Crocco temperature distribution being assumed (ref. 2), are shown in figure 4 in the form of velocity and pitot-pressure distributions for the centerbody plate mounted in the free stream and flush with the tunnel wall. The effect of various wall temperatures and Reynolds numbers on the boundary-layer profiles and thicknesses are also presented in figures 4 and 5, respectively. A comparison of the experimental profile data for a given set of conditions with the theoretical method of reference 3 is shown in both figures. The theory predicted the boundary-layer velocity and pitot-pressure profiles reasonably well but slightly underpredicted the boundary-layer thickness parameters.

Parametric Results

Experimental results of this investigation as a function of the geometric and aerodynamic parameters considered to be most important in inlet starting are presented in figure 6. Note that contraction ratio is a function of cowl bluntness since h_1 is measured from the stagnation point on the cowl leading edge. It can be seen from figure 6

that it is difficult to determine the relative importance of geometric and aerodynamic variables on the starting of hypersonic inlets, and no simple parameter was found which correlated the data with contraction ratio or relative inlet height. Extensive testing is required to obtain results in this form and they are useful only in the design of inlets which have very similar geometric characteristics and operate at virtually the same aerodynamic conditions. Results in this form contribute little, if any, to the understanding of the fundamentals of starting phenomena; therefore, starting was examined from a basic fluid mechanics approach.

Effect of Separation

The present investigation indicates that, for started configurations at near minimum inlet heights, both attached and separated flows occur. Figure 7 presents examples of started configurations both with little, if any, separation (fig. 7(a)) and with separation on the centerbody plate (fig. 7(b)). Although all details of the flow are not obvious from the schlieren photographs (due to large distortions produced by extreme pressure gradients), the major features of the flow field, including separation, become clearer when the photographs are used together with pressure distributions. Sketches of the flow patterns for two configurations shown in figure 7 together with the static-pressure distributions are presented in figure 8. The continuously increasing pressures along both surfaces for the configuration of figure 8(a) behave in the manner expected from a simple reflecting shock pattern associated with nonseparated flow. The pressure levels on both surfaces agree reasonably well with inviscid values. On the other hand, the successive increasing and decreasing pressures along the surfaces for the configuration of figure 8(b) denote the presence of expansions (dashed lines) as well as compressions (solid lines) within the passage. Of course the flow pattern presented in figure 8(b) is oversimplified in that it omits many shocks and expansions which are present as a result of the separated regions indicated on both walls. The presence of separation on the centerplate (due to the interaction of the bow shock from the cowl leading edge with the boundary layer) is indicated not only from the schlieren photographs but also from the pressure ratio on the centerplate at $x \approx 3$ cm. This value of pressure ratio (≈ 0.003) agrees with the first peak pressure for turbulent separation based on previous investigations (e.g., refs. 4 to 6). Approximately this same pressure ratio was obtained for almost every test with the model mounted in the free stream for blunt cowl leading-edge radii $\left(r_c/\delta = 0.075 \text{ and } 0.15\right)$ regardless of the cowl length l_c/δ, angle of attack α_c, or relative inlet height h_1/δ from 0.78 to 2.13; this indicated that separation occurred for all these started configurations. The reattachment of the boundary layer ahead of the throat was indicated from pitot pressures at the throat which did not show any reverse flow normally associated with separation.

The quantitative effect of the separation from the cowl shock on the inlet starting capability for the configuration in figure 7(b) with $h_1/h_2 = 2.33$ is not known. However,

the fact that the configuration did start with appreciable separation and a relatively large geometric contraction ratio, $h_1/h_2 = 1.98$ (the maximum theoretical starting contraction ratio from ref. 7 is only 1.44), indicates that this separation did not have a severely detrimental effect on the maximum starting contraction ratio. In fact, separation apparently had a beneficial effect on starting for this configuration; a similar behavior was observed in reference 8.

In view of these results, a reexamination of previous thinking on the effect of separation on the starting of hypersonic inlets is in order. The starting problem encountered with the early design of the HRE inlet model (ref. 1) was generally attributed, at least in part, to shock—boundary-layer interaction in the region of the cowl leading-edge station (ref. 3). Details of how and why this affects starting are not available – one possibility is that the cowl shock—boundary-layer separation produces aerodynamic choking. However, there appears to be a fallacy to this reasoning. If separation causes aerodynamic choking, it seems logical to conclude that the strong transient starting shock would have a more detrimental effect than the cowl shock. For example, when the transient shock is near the geometric throat, its resulting separation would increase the effective contraction ratio more than the separation produced by the cowl shock. (See ref. 9 for examples of separation caused by the transient starting shock.) Of course, a detrimental effect of the cowl shock on contraction ratio would occur when the separation bubble from the cowl shock merges in the vicinity of the geometric throat with the separation from the starting transient shock. This reasoning, along with the present data showing started inlets with separation in the vicinity of the cowl lip, indicates that separation caused by the cowl shock—boundary-layer interaction does not, in general, govern starting by adversely affecting the contraction ratio. However, the separation produced by the cowl shock is important in that during the transient starting period it increases the viscous losses through mixing as well as decreases the shock losses by reducing the strength of the shock system and, thereby, significantly affects the inlet pressure recovery. The importance of pressure recovery on starting is shown subsequently.

Pressure Recovery

Effect of pressure recovery on starting.- The importance of pressure recovery in the starting of supersonic diffusers is well known and has been demonstrated from a one-dimensional adiabatic flow analysis, with negligible back pressure being assumed (e.g., refs. 10 and 11). This simplified analysis shows that for a supersonic wind tunnel incorporating a second minimum or for a fixed-geometry inlet (fig. 9(a)), starting is a function of total-pressure recovery $p_{t,2}/p_{t,1}$, contraction ratio A_1/A_2 or h_1/h_2, and Mach number M_1. Since the maximum contraction ratio for starting is obtained when the flow at the second minimum is sonic, these parameters can be expressed by

$$\frac{A_1}{A_2} = \frac{A_1}{A^*} \frac{p_{t,2}}{p_{t,1}} \tag{1}$$

and their variation is shown in figure 9(b). Agreement between measured pressure recoveries and those predicted by one-dimensional theory (assuming inviscid flow) required for starting supersonic tunnels have been found in previous investigations (refs. 12 to 14). It should be noted that the required total-pressure recoveries shown in figure 9(b) are not limited to shock losses. Nevertheless, the starting criterion for supersonic inlets, having generally been discussed with emphasis on contraction ratio with a normal shock loss being assumed at the inlet face Mach number, is representative of the maximum internal losses. The curve for this criterion, generally referred to as the Kantrowitz criterion from reference 7, is shown in figure 9(b) as the dashed curve. This approach has been successful for current supersonic inlets since the viscous losses were relatively small due primarily to the thin boundary-layer thickness relative to the inlet height. However, for inlets with thick boundary layers relative to the inlet height (such as the HRE inlet of ref. 1), the viscous losses may be large and may result in total-pressure recovery less than for a normal shock and even less than that required for starting. It can be seen in figure 9(b) that in order to start even a constant-area duct $(A_1/A_2 = 1)$, the total-pressure recovery cannot be below a certain minimum for a given inlet Mach number – a point easily overlooked in inlet design.

Since the inlet total-pressure recovery governs when the passage will start, an analysis of the starting process requires an examination of the pressure recovery for the conditions just prior to the establishment of sonic velocity at the exit or throat. Consider the hypothetical, transient flow model, shown in figure 10(a) which has subsonic flow just upstream of the exit. This passage could not start if the inlet total-pressure recovery is less than that required in figure 9(b). This hypothetical flow pattern cannot be examined experimentally since the shock to subsonic flow will not move to this position unless the passage will start, and the complexity of such a flow field precludes any theoretical analysis at present. However, an experimental examination can be made for a started passage (figs. 10(b) and 10(c)) for which it can be reasoned that the inlet total-pressure recovery would be equal to or greater than that for the assumed transient condition. To illustrate this, a mass-weighted total-pressure recovery $\overline{p}_{t,2}/\overline{p}_{t,1}$ of only 0.08 was measured for a started inlet configuration with $\alpha_c = 0^\circ$, $r_c/\delta = 0.075$, and $\overline{M}_1 = 4.1$. Since this total-pressure recovery is below that required for starting this configuration, as seen in figure 9(b), this inlet passage should not be expected to start. In fact, after this passage was unstarted by closing the flap at the exit, the inlet, as predicted, failed to restart upon reopening the flap. (The inlet was initially started with precooled model walls. The restart attempt was made at near adiabatic wall conditions.)

Additional experimental results of two-dimensional inlet configurations with other cowl leading-edge radii (fig. 11(a)) show that when the mass-weighted total-pressure recovery was above that required by the one-dimensional (1-D) analysis, the inlet did restart (open symbols) after the throat flap was reopened. Also presented in figure 11(a) are results for these inlets, with measured pressure recoveries below those required by the analysis which did not start (solid symbols) or after the flap was reopened did not restart (tailed symbols). Results for other cowl angles of attack, presented in figures 11(b) and 11(c), also show that the measured total-pressure recoveries for all started configurations were above the required values calculated from the one-dimensional analysis. Thus, this one-dimensional analysis using a mass-weighted inlet Mach number gives a good estimate of the inlet total-pressure recovery required for starting these inlet configurations.

The required starting pressure recovery calculated from the one-dimensional analysis approaches the same value as the normal-shock pressure recovery for nearly all configurations with an inlet height more than about twice the boundary-layer thickness. (See fig. 11.) This accounts partially for the successful use in the past of the usual starting criterion based on normal shock loss since current supersonic inlets have inlet heights considerably greater than twice the boundary-layer thickness. It should be noted that the normal-shock pressure recovery and the required one-dimensional total-pressure recovery may also be the same at values of h_1/δ less than 2. (See figs. 11(b) and 11(c).)

Effect of parameters on pressure recovery.- The pressure recovery and therefore starting for this type inlet is sensitive to many design parameters. The data of figure 11 show that, for all configurations, the pressure recovery is extremely sensitive to small changes in the relative inlet height h_1/δ. Thus, the relative inlet height must be considered as well as contraction ratio for starting criteria. The use of only contraction ratio can be completely erroneous. For example, figure 6(a) shows that cowl bluntness has essentially no effect on the experimental maximum starting contraction ratio h_1/h_2 at $\alpha_c = 0^o$, but it does have a significant effect on the minimum relative inlet height h_1/δ required for starting. The maximum starting contraction ratios measured for these configurations are considerably below the allowable contraction ratios based on a normal shock at the mass-weighted inlet Mach number $\overline{M}_1$.

Although the effects of l_c/δ, r_c/δ, and α_c on pressure recovery can be seen in figure 11, a more informative method of examining the effects of these variables is presented in figure 12. When the length of the passage is short relative to the boundary-layer thickness $(l_c/\delta \leq 6)$, the pressure recovery is not affected greatly by changes in any of the other parameters. With increasing relative inlet length and the associated viscous losses, the effect on the pressure recovery by the other parameters becomes significantly larger; the pressure recovery decreases considerably with decreasing inlet height (especially for

$h_1/\delta \leq 1$, fig. 12(a)), with increasing cowl bluntness (particularly for $r_c/\delta \geq 0.075$, fig. 12(b)), and with increasing cowl angle (noticeably for $\alpha_c \geq 4^o$, fig. 12(c)). It is only at the larger cowl lengths $(l_c/\delta \geq 10)$ that the measured pressure recovery approaches values which the one-dimensional analysis indicates are critical in determining whether or not a passage will start. From these results it can be seen that the design conditions for the HRE inlet of reference 1 $(l_c/\delta \approx 12, \quad r_c/\delta \approx 0.10, \quad h_1/\delta \approx 1.0, \quad \alpha_c \approx 5^o)$ place it in the critical area for which starting would be expected to be marginal, at best. In the critical starting region the parameters shown in figure 12 quite apparently have a strong interdependence.

The pressure recovery is seen in figure 12(d) to be essentially independent of Reynolds number for these large turbulent intake boundary layers. Although only limited data on the effect of wall cooling were obtained, figure 12(d) indicates that decreasing the wall temperature results in increasing the pressure recovery and, thus, would be expected to have a favorable effect on starting. A similar favorable effect on starting by wall cooling was found in references 1 and 3. It should be noted that the pressure recovery increased only slightly with wall cooling (fig. 12(d)) because the inlet height was reduced to maintain a constant h_1/δ. However, for the same inlet height, the favorable effect on pressure recovery would be greater because h_1/δ would increase. (See fig. 12(d).) In reality, wall cooling thins the boundary layer and, therefore, the pressure recovery increases for the given inlet height. Since this pressure recovery is also a function of the ratios of cowl length and cowl bluntness to boundary-layer thickness, each of these ratios must also be considered in determining pressure recovery and starting.

The data presented in figure 12 are in the form which can be useful in any future method to predict pressure recovery; and it appears that the prediction of pressure recovery is mandatory for the prediction of starting for these type inlets.

Basic Data

Some of the basic data (static and pitot pressure distribution, schlieren photographs, and mass-weighted Mach numbers and total pressure) which were used to formulate the foregoing results are presented in figures 13 to 16.

CONCLUSIONS

An investigation has been conducted on the starting phenomena for hypersonic inlets with relatively thick intake turbulent boundary layers at a free-stream Mach number of 6. The effects on starting of cowl bluntness, cowl length, cowl angle of attack, boundary-layer thickness, free-stream Reynolds number, and wall temperature have been examined and the following conclusions are made:

1. Inlet total-pressure recovery (including both shock and viscous losses) is the governing factor determining starting in contrast to only normal-shock pressure recovery usually considered.

2. The total-pressure recovery required for starting is predicted reasonably well by a one-dimensional analysis. In general, the usual method of assuming only a normal-shock pressure recovery is applicable to inlets with sufficiently large inlet heights h_1 relative to boundary-layer thickness δ which for present configurations corresponded to $h_1/\delta \geq 2$.

3. Total-pressure recovery is extremely sensitive to small changes in the ratio of inlet height to boundary-layer thickness $\left(h_1/\delta \lessapprox 2\right)$ and, therefore, the choice of this ratio is critical for starting.

4. Boundary-layer separation in the vicinity of the cowl lip station affects starting in that it decreases the shock losses but increases the viscous losses through mixing. However, this separation does not generally govern starting by adversely affecting contraction ratio.

5. With increasing cowl length l_c relative to the boundary-layer thickness $\left(\text{especially for } l_c/\delta \geq 10\right)$, the pressure recovery becomes more adversely affected by decreasing relative inlet height, increasing cowl bluntness, and increasing cowl angle. These parameters are interrelated with the relative importance of one a strong function of the others.

6. The pressure recovery is essentially independent of Reynolds number (except as it affects the boundary-layer thickness).

7. Wall cooling has a favorable effect on starting. For a constant h_1/δ, obtained by varying h_1, the pressure recovery increases slightly. Indications are that wall cooling primarily thins the boundary layer and, therefore, the pressure recovery increases significantly for a constant h_1.

8. Any future theoretical method of predicting the starting of hypersonic inlets will be dependent upon the prediction of total-pressure recovery which must account for separation and viscous losses due to mixing as well as internal shock losses. The present investigation provides data which can be used to verify future theoretical or empirical methods for predicting pressure recovery and thus starting.

Langley Research Center,
National Aeronautics and Space Administration,
Hampton, Va., June 21, 1971.

APPENDIX

DESCRIPTION AND CALIBRATION OF THE LANGLEY 20-INCH MACH 6 TUNNEL

By James C. Emery
Langley Research Center

SYMBOLS

M	Mach number
ΔM	difference between Mach number of rake and fixed probe, $M_r - M_p$
p	pressure, MN/m^2
s'	inside measurement of tunnel in vertical and horizontal planes (see fig. A4), cm
T	temperature, K
x'	distance measured along longitudinal axis of tunnel from center line of upstream window (positive in upstream direction, see fig. A4), cm
μ	viscosity, N sec/m^2
ϕ	rake angle: horizontal, 0^o; vertical, 90^o

Subscripts:

a	average (always calculated within the core given in table AII)
p	fixed probe (see fig. A4)
r	rake probe
t	total or stagnation
1	condition in settling chamber
2	condition behind normal shock

APPENDIX

Facility Description

The Langley 20-inch Mach 6 tunnel is a blowdown type with air as the test medium. Figure A1 schematically shows the general arrangement of this facility in which heat-transfer, pressure, and force tests are conducted. The test Mach number is achieved with a fixed-geometry two-dimensional contoured nozzle (side walls are parallel) forming a throat section of 0.86 by 50.80 cm and a test section of 52.00 by 50.80 cm. The nozzle length from the throat to the tunnel window center line measures 2.27 m.

Models can be mounted either in a fixed position on the tunnel floor or on injection systems at top and bottom of the tunnel test section. The opening in the bottom of the test section measures approximately 132 by 40 cm for the lower injection system which includes a remote controlled sting-support system capable of moving the model, during wind-on operation, through an angle-of-attack range from -5° to 55° and a side-slip angle range from 0° to -10°. For heat-transfer tests, the lower injection system traverses the last 25 cm in approximately 0.3 sec with a maximum acceleration of 6g (1g = 9.807 m/sec^2). For force tests, the model can also be injected to reduce starting and unstarting loads. For this type of test the injection time for the last 25 cm is adjusted to about 0.9 sec with a maximum 2g acceleration. Details of the lower model injection system including sting support are shown in figure A2. The top injection system, with a usable opening of 50 by 36 cm and a similar injection rate, is used primarily for heat-transfer tests since the model attitude cannot be changed during wind-on operation. The top injection-system opening and mounting plate are shown in figure A3. A reference Mach number is obtained from a fixed pitot probe mounted in the upper wall of the test section as shown in figure A4.

The tunnel has a movable second minimum and exhausts either into the atmosphere with the aid of an annular air ejector or into a vacuum sphere. The tunnel can exhaust to the vacuum sphere and through the ejector simultaneously. This mode of operation is frequently used with force tests to reduce starting and unstarting loads. Tunnel operating conditions are as follows:

Stagnation pressure	0.21 MN/m^2 to 3.62 MN/m^2
Stagnation temperature	450 K to 560 K
Reynolds number	2.3×10^6/m to 29.5×10^6/m
Dynamic pressure	3.35 kN/m^2 to 57.8 kN/m^2
Running time (maximum):	
With sphere	2 min
With ejector	20 min
Tunnel mass flow (maximum)	27 kg/sec
Ejector mass flow	60 to 80 kg/sec

APPENDIX

Tunnel air, heated by an electrical resistance heater, is supplied from a 4.1 MN/m^2 tank field with a storage capacity of 3780 m^3 (186 000 kg). The pumps for this field operate at a rate of 21 kg/sec and an activated alumina dryer provides a dewpoint temperature of 233 K at a pressure of 4.1 MN/m^2. One hundred analog channels and seven digital channels of data can be recorded on a central data recording complex.

Mach Number Calibration

This facility was calibrated by using a 19-tube rake with tubes spaced 2.54 cm apart, placed at four stations along the test-section axis. Calibrations were made for both vertical and horizontal positions at each station for four stagnation pressures ranging from 0.5 MN/m^2 to 3.0 MN/m^2.

Previous tunnel calibrations had shown that the Mach number varied with time (time during each run, the time between runs, and total elapsed time) probably as a result of temperature effects on the boundary layer and nozzle. This phenomenon makes it extremely difficult to obtain an exact calibration curve of Mach number, since all rake positions could not be taken simultaneously; therefore, the variation in test-section Mach number ΔM is presented as the difference between the Mach numbers calculated from the rake pitot pressures and the fixed-probe pitot pressures. In addition, to further minimize temperature differences between runs, the interior walls of the test section were preheated to 325 K prior to each survey. Desired test conditions were then established and data were taken at various pressures within a time interval of 3 to 5 min.

The Mach number distributions determined from the measured pressures on the rake and fixed position probe are presented for each axial station and test condition in table AI. The variation in test-section Mach number ΔM obtained from these data is presented in figure A5 along with the Mach number for the fixed probe.

For convenience in determining the practical size of models to be tested in this facility, the variation in the test core size with pressure and axial station is shown in figure A6. These cores were obtained from the data of table AI or figure A5 and represent the region where the maximum Mach number variation was approximately ± 0.02 in the horizontal and vertical planes. The average values of ΔM within each core are given in figure A7 and table AII. Figure A7 suggests a possible fairing of these averages. The average Mach number at any station may be determined by adding ΔM_a to the measured probe Mach number. This method assumes the same effect of temperature on Mach number at each point in the test section. Figure A8 illustrates how the Mach number differential for two repeat runs decreases when the rake Mach numbers are referred to the fixed probe.

The Reynolds number for various temperatures and pressures is presented in figure A9. Also shown are the values of the pressures and temperatures for liquefaction obtained from reference 15 and the viscosity relationship from reference 16.

REFERENCES

1. Henry, J. R.; Andrews, E. H., Jr.; Pinckney, S. Z.; and McClinton, C. R.: Boundary Layer and Starting Problems on a Short Axisymmetric Scramjet Inlet. Compressible Turbulent Boundary Layers, NASA SP-216, 1968, pp. 481-508.

2. Schlichting, Hermann (J. Kestin, transl.): Boundary Layer Theory. Fourth ed., McGraw-Hill Book Co., Inc., c.1960, p. 346.

3. Andrews, Earl H., Jr.; McClinton, Charles R.; and Pinckney, S. Z.: Flow Field and Starting Characteristics of an Axisymmetric Mixed Compression Inlet. NASA TM X-2072, 1971.

4. Chapman, Dean R.; Kuehn, Donald M.; and Larson, Howard K.: Investigation of Separated Flows in Supersonic and Subsonic Streams With Emphasis on the Effect of Transition. NACA Rep. 1356, 1958. (Supersedes NACA TN 3869.)

5. Sterrett, James R.; and Emery, James C.: Extension of Boundary-Layer-Separation Criteria to a Mach Number of 6.5 By Utilizing Flat Plates With Forward-Facing Steps. NASA TN D-618, 1960.

6. Goldberg, Theodore J.: Turbulent Separation Associated With Axisymmetric Flared Bodies. J. Spacecraft Rockets, vol. 4, no. 11, Nov. 1967, pp. 1551-1553.

7. Kantrowitz, Arthur; and Donaldson, Coleman duP.: Preliminary Investigation of Supersonic Diffusers. NACA WR L-713, 1945. (Formerly NACA ACR L5D20.)

8. Mitchell, Glenn A.; and Cubbison, Robert W.: An Experimental Investigation of the Restart Area Ratio of a Mach 3.0 Axisymmetric Mixed Compression Inlet. NASA TM X-1547, 1968.

9. Moore, John A.: Investigation of the Effect of Short Fixed Diffusers on Starting Blowdown Jets in the Mach Number Range From 2.7 to 4.5. NACA TN 3545, 1956.

10. Shapiro, Ascher H.: The Dynamics and Thermodynamics of Compressible Fluid Flow. Vol. I. Ronald Press Co., c.1953, pp. 144-145.

11. Liepmann, Hans Wolfgang; and Puckett, Allen E.: Introduction to Aerodynamics of a Compressible Fluid. John Wiley & Sons, Inc., 1947, pp. 70-71.

12. Neumann, E. P.; and Lustwerk, F.: Supersonic Diffusers for Wind Tunnels. J. Appl. Mech., vol. 16, no. 2, June 1949, pp. 195-202.

13. Diggins, J. L.; and Lange, A. H.: A Systematic Study of a Variable Area Diffuser for Supersonic Wind Tunnels. NAVORD Rep. 2421, U.S. Naval Ord. Lab. (White Oak, Md.), Dec. 1952.

14. Wegener, Peter P.; and Lobb, R. Kenneth: NOL Hypersonic Tunnel No. 4 Results II: Diffuser Investigation. NAVORD Rep. 2376, U.S. Naval Ord. Lab. (White Oak, Md.), May 5, 1952.

15. Buhler, R. D.; and Nagamatsu, H. T.: Condensation of Air Components in Hypersonic Wind Tunnels – Theoretical Calculations and Comparison With Experiment. GALCIT Mem. No. 13 (Contract No. DA-04-495-Ord-19), Dec. 1, 1952.

16. Bertram, Mitchel H.: Comment on "Viscosity of Air." J. Spacecraft Rockets, vol. 4, no. 2, Feb. 1967, p. 287.

TABLE AI.- MACH NUMBER CALCULATED FROM $p_{t,2}/p_{t,1}$

(a) $p_{t,1} = 0.52$ MN/m^2; $T_{t,1} = 478$ K

s', cm	M for –							
	x' = 21.59 cm		x' = 1.59 cm		x' = -25.40 cm		x' = -55.88 cm	
	$\phi = 0^o$	$\phi = 90^o$	$\phi = 0^o$	$\phi = 90^o$	$\phi = 0^o$	$\phi = 90^o$	$\phi = 0^o$	$\phi = 90^o$
22.86	8.24	7.57	8.72	7.54	----	7.48	----	7.44
20.32	6.15	6.26	6.57	6.29	6.98	6.07	7.73	6.28
17.78	5.96	6.00	5.78	5.98	5.89	5.86	6.06	5.97
15.24	5.94	5.98	5.92	5.97	5.87	5.86	5.92	6.00
12.70	5.92	5.97	5.93	5.93	5.91	5.88	5.94	5.75
10.16	5.91	5.95	5.94	5.91	5.90	5.89	5.92	5.96
7.62	5.91	5.93	5.94	5.91	5.89	5.89	5.96	5.97
5.08	5.91	5.90	5.93	5.92	5.91	5.90	5.98	5.89
2.54	5.88	5.90	5.92	5.91	5.91	5.90	5.97	5.98
0	5.88	5.91	5.91	5.92	5.91	5.90	5.97	5.99
-2.54	5.88	5.90	5.92	5.91	5.91	5.89	5.98	5.98
-5.08	5.91	5.91	5.93	5.91	5.90	5.90	5.97	5.98
-7.62	5.91	5.93	5.95	5.91	5.90	5.89	5.94	5.97
-10.16	5.92	5.96	5.94	5.91	5.90	5.89	5.94	5.93
-12.72	5.92	5.98	5.93	5.91	5.92	5.87	5.95	5.94
-15.24	5.97	5.99	5.91	5.93	5.89	5.83	5.94	5.97
-17.78	5.97	6.01	5.95	5.97	5.99	5.86	6.37	5.95
-20.32	6.83	----	7.26	6.31	7.78	6.17	8.30	6.25
-22.86	8.96	7.58	----	7.54	----	7.28	----	7.29
M_p	5.912	5.944	5.941	5.944	5.905	5.890	5.953	5.960

(b) $p_{t,1} = 1.14$ MN/m^2; $T_{t,1} = 478$ K

s', cm	M for –							
	x' = 21.59 cm		x' = 1.59 cm		x' = -25.40 cm		x' = -55.88 cm	
	$\phi = 0^o$	$\phi = 90^o$	$\phi = 0^o$	$\phi = 90^o$	$\phi = 0^o$	$\phi = 90^o$	$\phi = 0^o$	$\phi = 90^o$
22.86	8.09	7.27	8.46	7.26	8.94	7.26	----	7.00
20.32	6.05	6.06	6.20	6.10	6.65	6.01	7.33	5.97
17.78	6.02	6.02	5.95	5.99	5.96	5.94	5.98	6.06
15.24	6.00	6.01	5.95	5.98	5.97	5.94	5.98	5.93
12.70	5.99	5.99	5.95	5.94	5.98	5.95	5.99	5.96
10.16	5.98	5.98	5.95	5.92	5.97	5.96	5.99	6.00
7.62	5.98	5.96	5.96	5.92	5.97	5.97	6.02	6.00
5.08	5.97	5.93	5.94	5.92	5.97	5.96	6.03	5.97
2.54	5.95	5.93	5.93	5.92	5.99	5.97	6.04	6.01
0	5.95	5.95	5.93	5.92	5.98	5.97	6.04	6.01
-2.54	5.96	5.93	5.93	5.92	5.98	5.96	6.04	6.01
-5.08	5.98	5.95	5.93	5.93	5.98	5.97	6.03	6.01
-7.62	5.98	5.97	5.96	5.92	5.98	5.97	6.02	6.00
-10.16	5.98	5.99	5.96	5.93	5.97	5.96	6.00	5.97
-12.72	5.98	6.00	5.95	5.95	5.99	5.95	6.00	5.97
-15.24	6.03	6.01	5.93	5.99	5.96	5.93	6.01	5.99
-17.78	6.03	6.02	5.99	6.00	5.98	5.94	6.09	6.00
-20.32	6.47	----	6.88	6.08	7.50	6.09	8.02	6.04
-22.86	8.86	7.36	----	7.26	----	7.19	----	7.01
M_p	5.986	5.974	5.947	5.962	5.973	5.965	5.994	5.982

TABLE AI.- MACH NUMBER CALCULATED FROM $p_{t,2}/p_{t,1}$ – Concluded

(c) $p_{t,1} = 2.17$ MN/m^2; $T_{t,1} = 478$ K

s', cm	M for –							
	x' = 21.59 cm		x' = 1.59 cm		x' = -25.40 cm		x' = -55.88 cm	
	$\phi = 0^o$	$\phi = 90^o$	$\phi = 0^o$	$\phi = 90^o$	$\phi = 0^o$	$\phi = 90^o$	$\phi = 0^o$	$\phi = 90^o$
22.86	7.71	7.03	8.11	6.94	8.69	7.00	----	6.81
20.32	6.04	6.02	6.06	6.05	6.39	6.02	6.99	5.99
17.78	6.04	6.04	5.98	6.01	5.98	5.97	5.98	6.12
15.24	6.03	6.03	5.98	6.01	6.00	5.97	6.00	5.91
12.70	6.02	6.02	5.98	5.97	6.00	5.98	6.00	5.99
10.16	6.01	6.01	5.99	5.95	6.00	5.99	6.01	6.03
7.62	6.00	5.99	5.98	5.95	5.99	5.99	6.03	6.03
5.08	5.99	5.96	5.96	5.96	6.00	5.99	6.03	6.02
2.54	5.98	5.95	5.96	5.96	6.02	5.99	6.04	6.04
0	5.98	5.98	5.95	5.96	6.01	6.00	6.04	6.04
-2.54	5.99	5.97	5.96	5.96	6.01	5.99	6.05	6.03
-5.08	6.00	5.97	5.96	5.96	6.00	6.00	6.03	6.04
-7.62	6.00	5.99	5.99	5.95	6.00	6.00	6.03	6.03
-10.16	6.02	6.01	5.98	5.96	6.00	5.99	6.01	6.02
-12.72	6.01	6.02	5.98	5.98	6.02	5.98	6.01	6.01
-15.24	6.05	6.03	5.97	6.01	5.99	5.98	6.03	6.03
-17.78	6.04	6.04	5.99	6.03	6.00	5.96	6.02	6.04
-20.32	6.01	6.04	6.54	6.02	7.16	6.04	7.68	6.03
-22.86	8.52	7.12	8.82	7.04	----	6.99	----	6.86
M_p	5.997	5.993	5.965	5.980	5.990	5.981	6.011	6.002

(d) $p_{t,1} = 3.03$ MN/m^2; $T_{t,1} = 478$ K

s', cm	M for –							
	x' = 21.59 cm		x' = 1.59 cm		x' = -25.40 cm		x' = -55.88 cm	
	$\phi = 0^o$	$\phi = 90^o$	$\phi = 0^o$	$\phi = 90^o$	$\phi = 0^o$	$\phi = 90^o$	$\phi = 0^o$	$\phi = 90^o$
22.86	7.48	6.95	7.90	6.89	8.49	6.94	8.92	6.77
20.32	6.04	6.02	6.03	6.05	6.26	6.03	6.79	6.02
17.78	6.05	6.05	5.99	6.02	5.98	5.97	5.99	6.11
15.24	6.03	6.03	5.98	6.01	6.01	5.97	6.01	5.91
12.70	6.02	6.02	5.97	5.99	6.00	5.98	6.00	5.99
10.16	6.00	6.02	5.98	5.96	6.00	5.99	6.01	6.02
7.62	6.00	5.99	5.98	5.96	5.99	5.99	6.03	6.03
5.08	5.99	5.97	5.96	5.97	6.00	5.99	6.03	6.03
2.54	5.98	5.96	5.96	5.96	6.01	5.99	6.04	6.04
0	5.99	5.98	5.95	5.96	6.01	5.99	6.04	6.04
-2.54	5.99	5.97	5.96	5.97	6.01	5.98	6.04	6.03
-5.08	5.99	5.98	5.95	5.96	6.00	5.99	6.03	6.04
-7.62	6.00	6.00	5.98	5.96	6.00	6.00	6.03	6.02
-10.16	6.02	6.02	5.98	5.97	5.99	5.99	6.01	6.02
-12.72	6.01	6.03	5.98	5.99	6.02	5.98	6.02	6.00
-15.24	6.05	6.04	5.96	6.02	5.99	5.99	6.03	6.03
-17.78	6.05	6.04	5.99	6.03	6.00	5.97	6.01	6.04
-20.32	6.15	6.03	6.39	6.02	6.99	6.05	7.48	6.05
-22.86	8.34	7.06	8.65	6.98	----	6.95	----	6.79
M_p	5.997	5.995	5.964	5.982	5.995	5.981	6.012	6.006

TABLE AII.- TUNNEL FLOW PARAMETERS

x', cm	$p_{t,2'}$, MN/m^2	ϕ, deg	M_p	ΔM	ΔM_a	Core size, cm
21.59	0.52	0	5.912	-0.007	-0.018	25
21.59	.52	90	5.944	-.032		16
1.59	0.52	0	5.941	-0.011	-0.020	33
1.59	.52	90	5.944	-.029		28
-25.40	0.52	0	5.905	-0.004	-0.004	33
-25.40	.52	90	5.890	-.004		31
-55.88	0.52	0	5.953	-0.001	+0.002	31
-55.88	.52	90	5.960	+.004		28
21.59	1.14	0	5.986	-0.013	-0.018	26
21.59	1.14	90	5.974	-.024		18
1.59	1.14	0	5.947	-0.002	-0.016	33
1.59	1.14	90	5.962	-.030		28
-25.40	1.14	0	5.973	+0.005	-0.002	36
-25.40	1.14	90	5.965	-.010		36
-55.88	1.14	0	5.994	+0.023	+0.017	28
-55.88	1.14	90	5.982	+.012		31
21.59	2.17	0	5.997	+0.001	-0.009	23
21.59	2.17	90	5.993	-.020		16
1.59	2.17	0	5.965	+0.009	-0.006	36
1.59	2.17	90	5.980	-.022		26
-25.40	2.17	0	5.990	+0.014	+0.009	36
-25.40	2.17	90	5.981	+.005		36
-55.88	2.17	0	6.011	+0.016	+0.020	28
-55.88	2.17	90	6.002	+.025		33
21.59	3.03	0	5.997	+0.002	-0.007	26
21.59	3.03	90	5.995	-.016		18
1.59	3.03	0	5.964	+0.006	-0.003	33
1.59	3.03	90	5.982	-.013		26
-25.40	3.03	0	5.995	+0.008	+0.005	36
-25.40	3.03	90	5.981	+.003		36
-55.88	3.03	0	6.012	+0.009	+0.013	36
-55.88	3.03	90	6.006	+.018		28

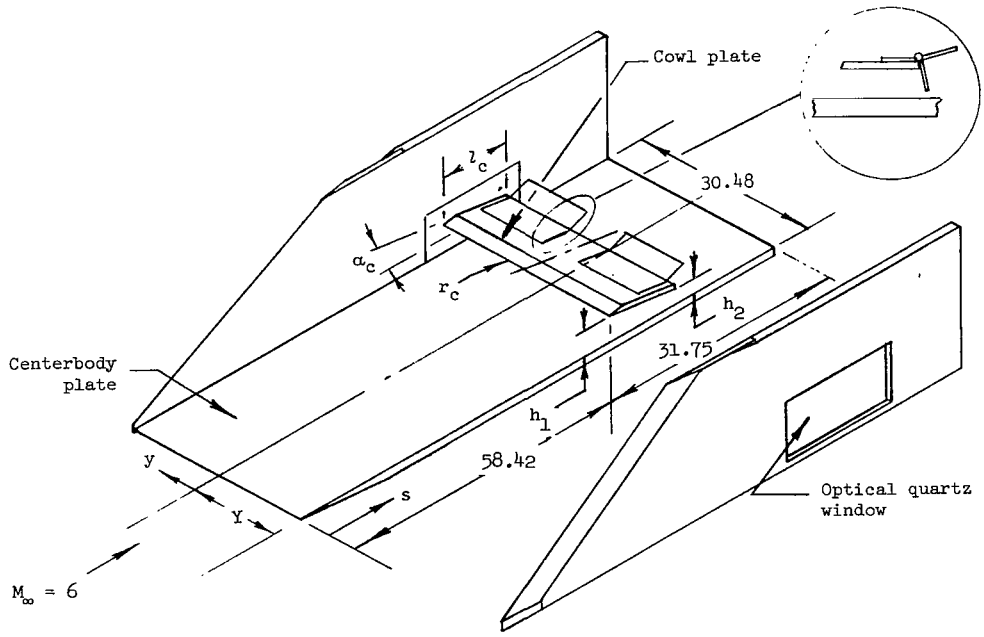

Centerbody plate

Pressure orifice locations

s	y	s	y	s	y
12.70	0	53.34	0	59.69	0
20.30	↓	54.60	↓	60.96	↓
27.94		55.88		63.50	
33.02		↓	± 6.35	66.04	
38.10			±12.70	68.58	
43.18		57.15	0	71.12	
48.26		58.42	0	73.66	
49.50		↓	± 6.35	76.20	
50.80			±10.16	81.28	
52.10	↓		±12.70	86.36	↓

Thermocouple locations

s	y
38.10	± 2.54
53.34	± 2.54
↓	±12.70
58.42	± 2.54

Cowl plate

Pressure orifice locations

Y = 0

l_c = 5.08

s
60.96
62.23

l_c = 10.16

s
60.96
62.23
63.50
64.77
66.04
67.31

l_c = 15.24

s
60.96
62.23
63.50
64.77
66.04
67.31
68.58
69.85
71.12
72.39

l_c = 30.48

s
60.96
63.50
66.04
68.58
71.12
76.20
81.28
86.36

l_c = 45.72

s
60.96
63.50
66.04
68.58
71.12
76.20
81.28
86.36
91.44
96.52

(a) Model mounted in free stream.

Figure 1.- Model and instrumentation. All dimensions are in cm.

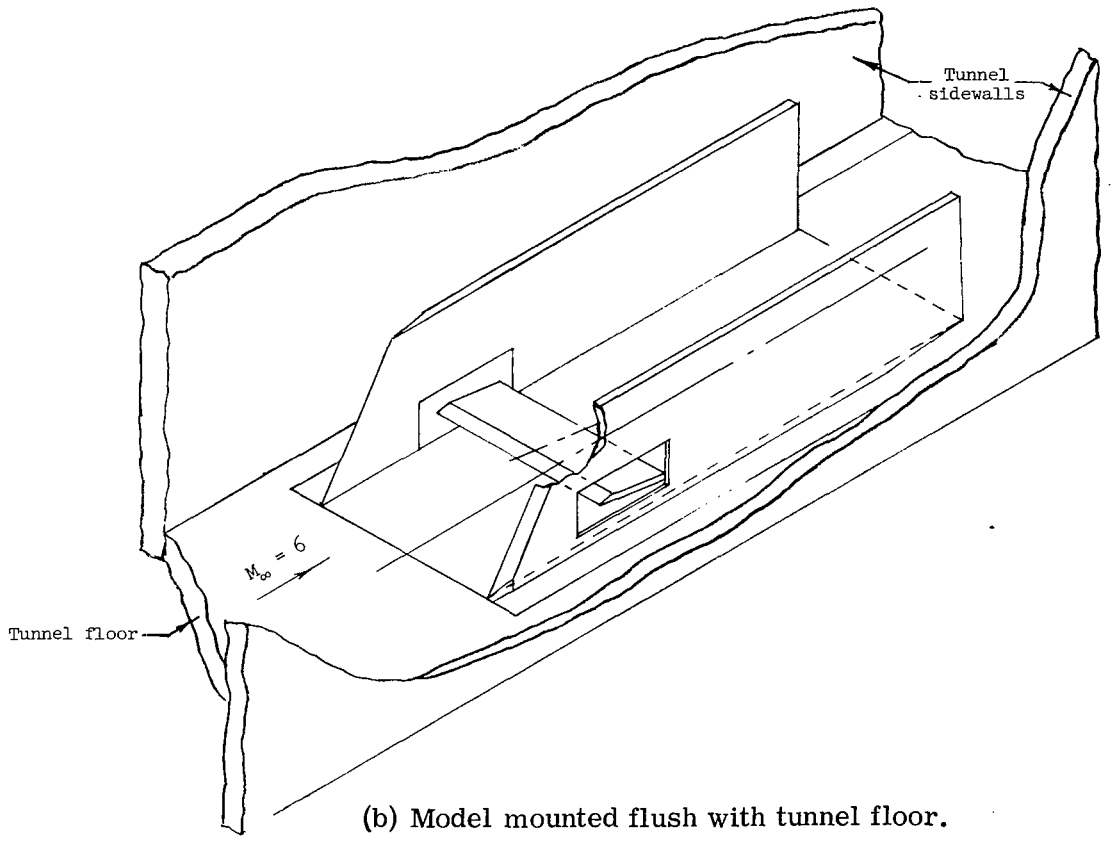

(b) Model mounted flush with tunnel floor.

Orifice no.	z	y	Tube I.D.	Tube O.D.
1	0.112	0.980	0.051	0.081
2	.224	.721		
3	.287	.493		
4	.376	.249		
5	.470	.000		
6	.718			
7	1.050			
8	1.550		.102	.152
9	2.060			
10	2.580			
11	3.080			
12	3.590			
13	4.100			
14	4.610			
15	5.100			

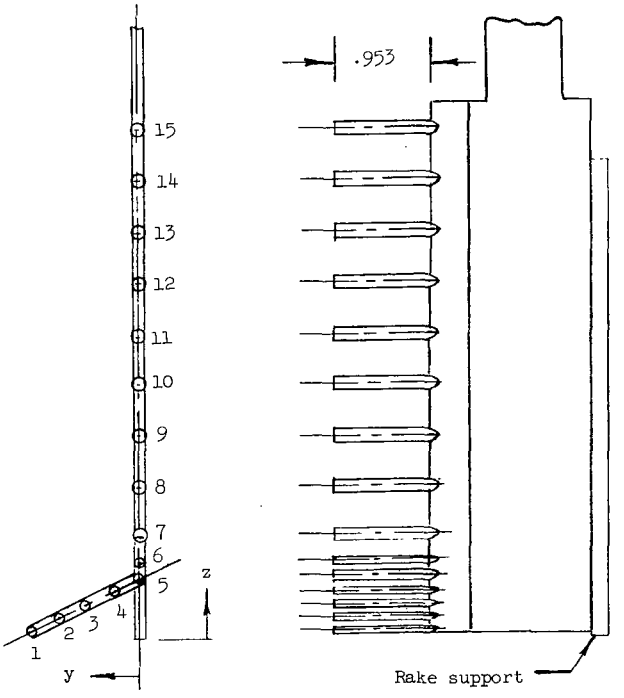

(c) Details of survey rake.

Figure 1.- Concluded.

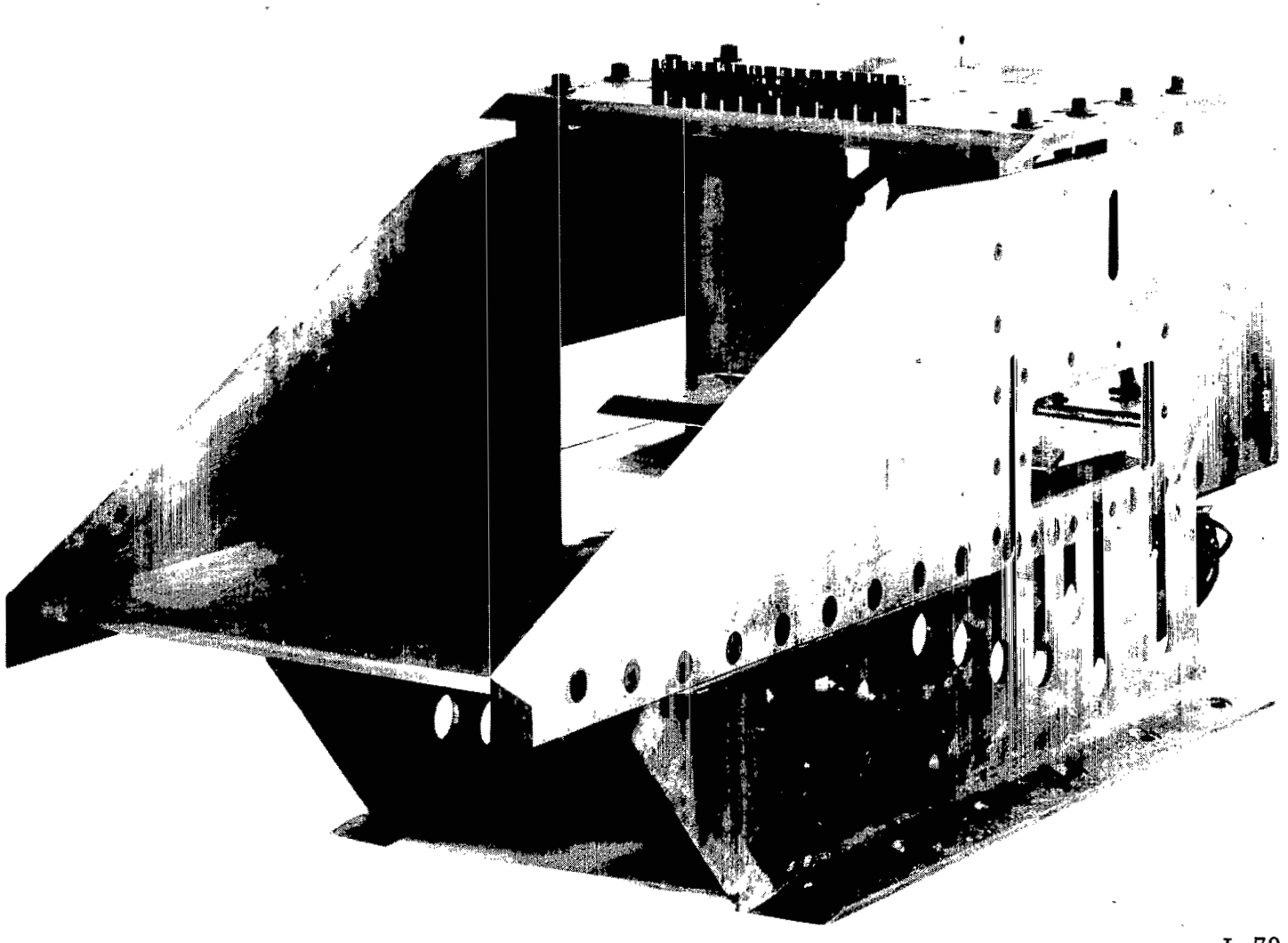

L-70-4074

Figure 2.- Two-dimensional inlet model.

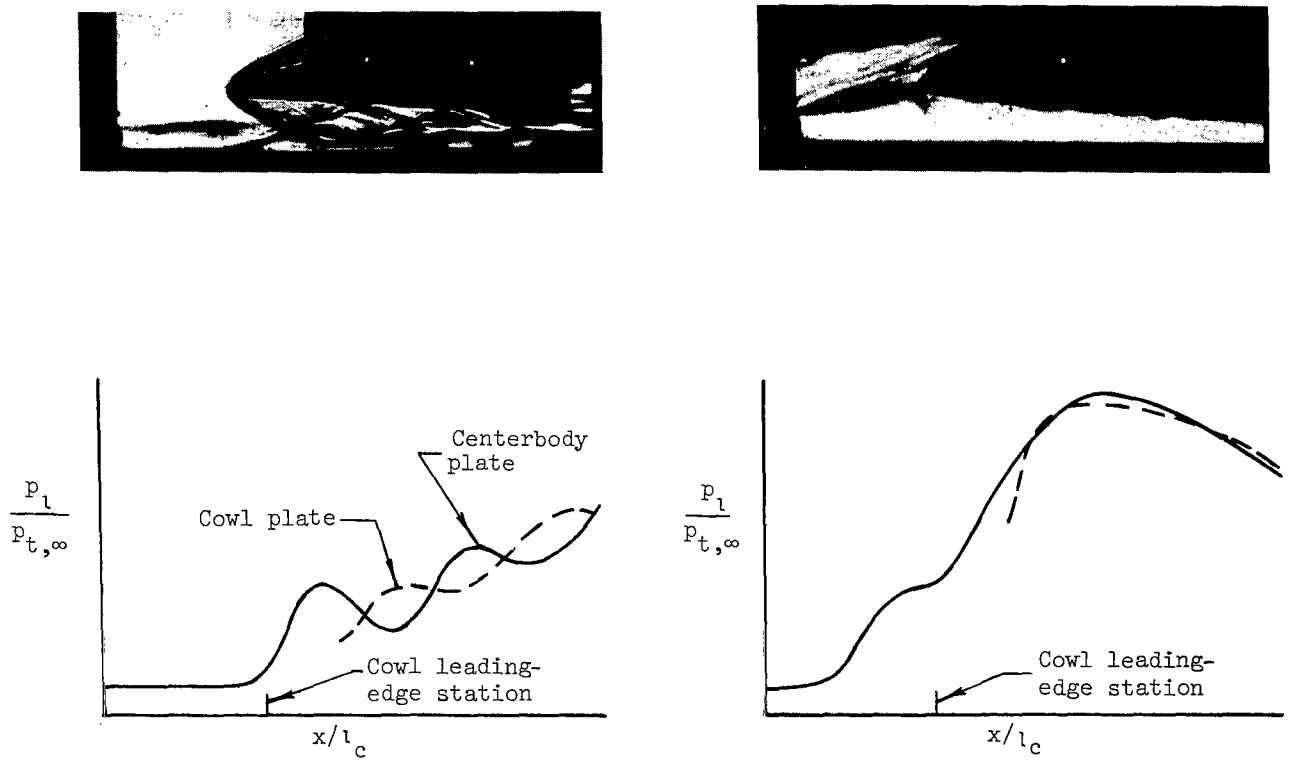

(a) Started. (b) Unstarted.

Figure 3.- Typical schlieren photographs and pressure distributions used to determine inlet start and unstart.

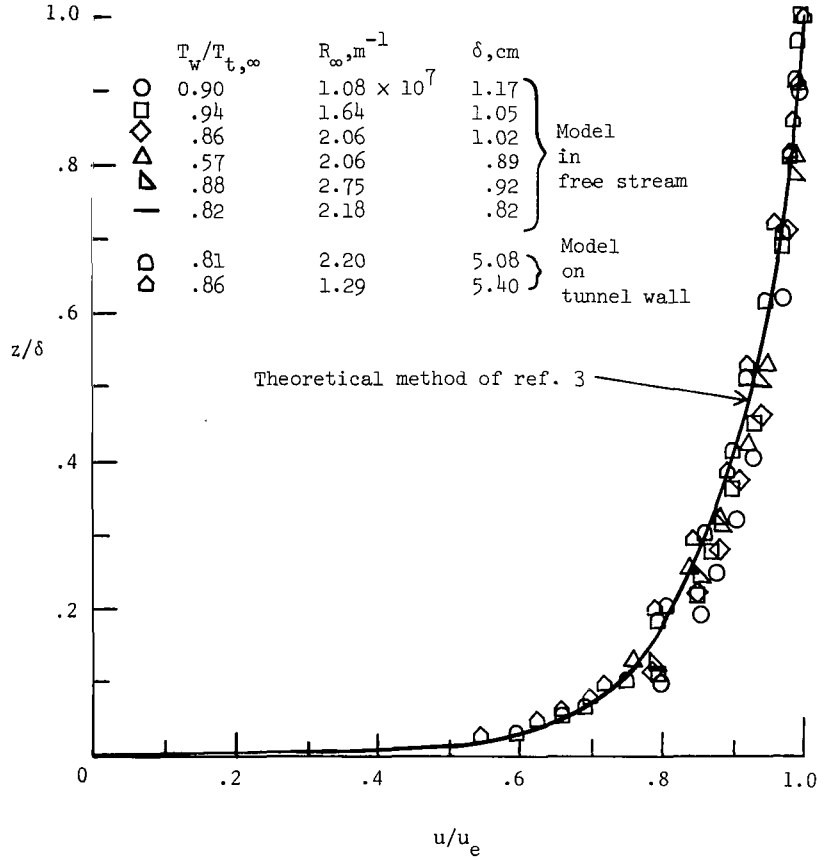

(a) Velocity distribution.

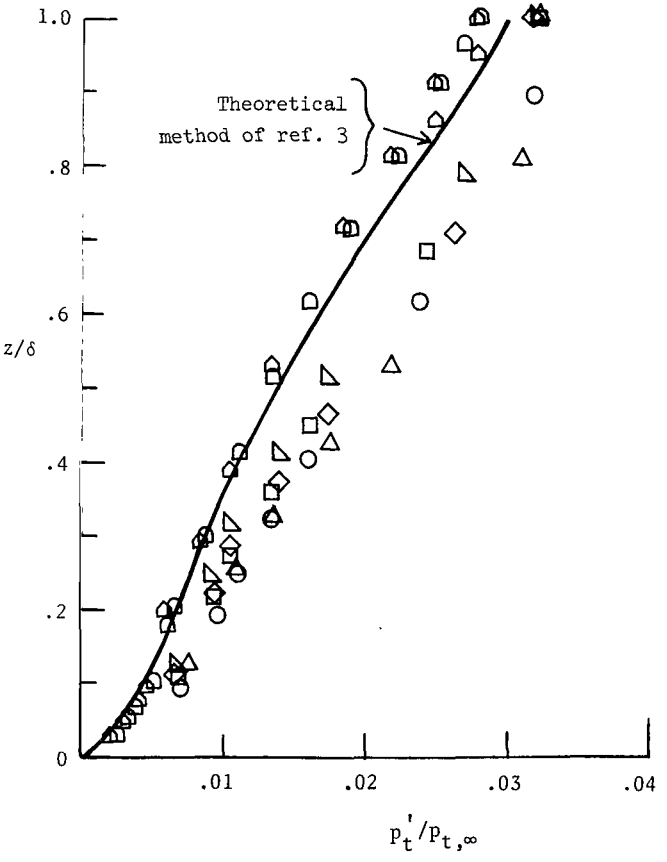

(b) Pitot-pressure distribution.

Figure 4.- Boundary-layer profiles at the cowl lip station.

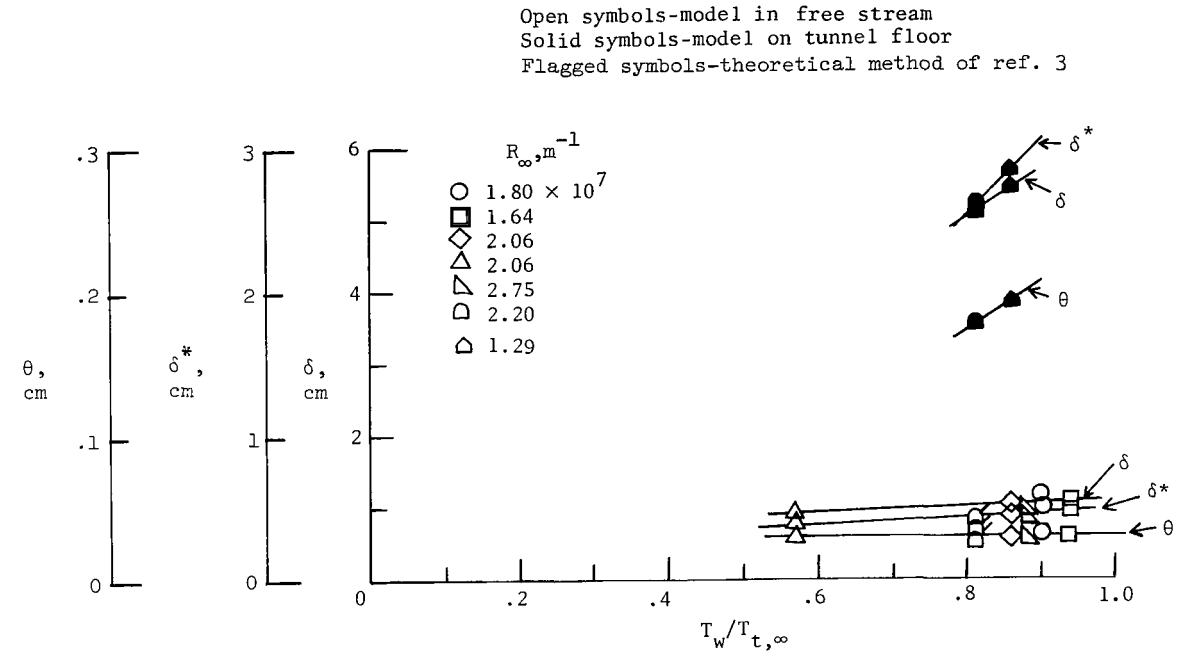

(a) Effect of wall temperature.

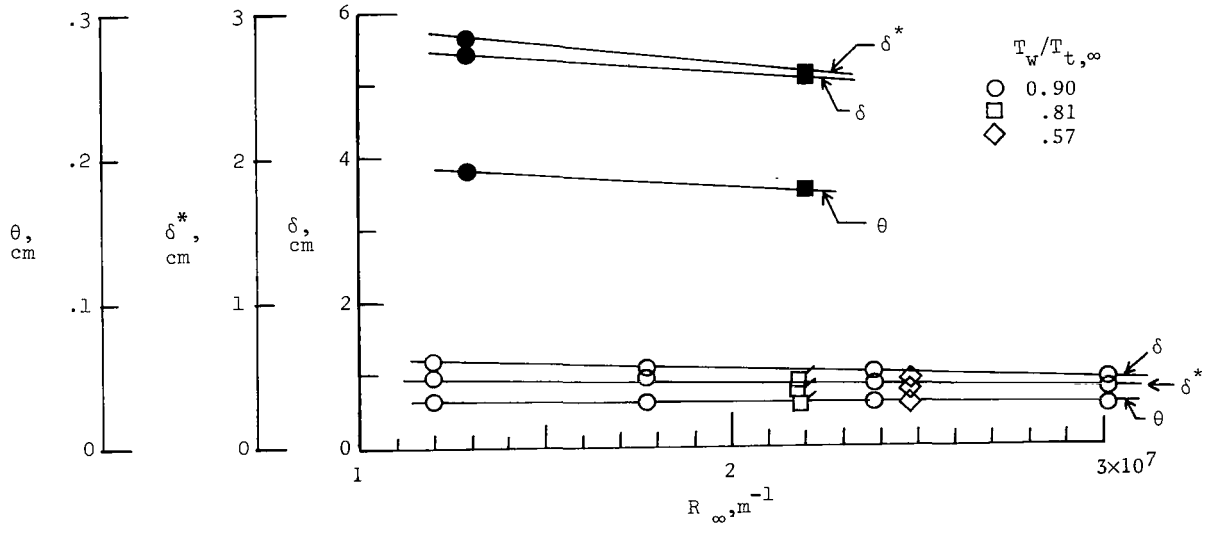

(b) Effect of unit Reynolds number.

Figure 5.- Turbulent-boundary-layer characteristics as a function of Reynolds number and wall temperature.

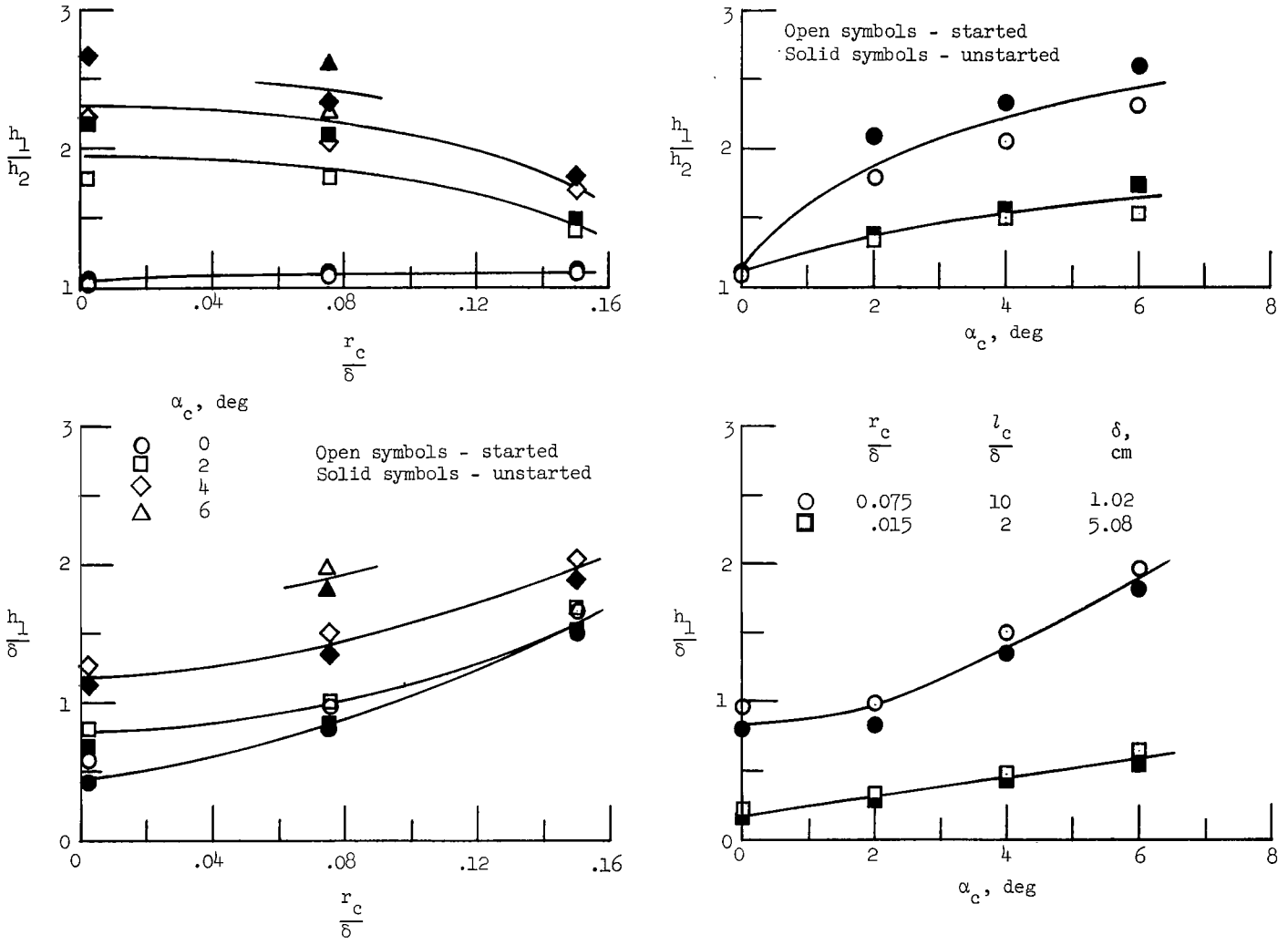

(a) Effect of cowl bluntness. $l_c/\delta = 10$; $\delta = 1.02$ cm.

(b) Effect of cowl angle of attack.

Figure 6.- Required relative inlet height and contraction ratio for starting. $R_\infty = 2.06 \times 10^7$/m.

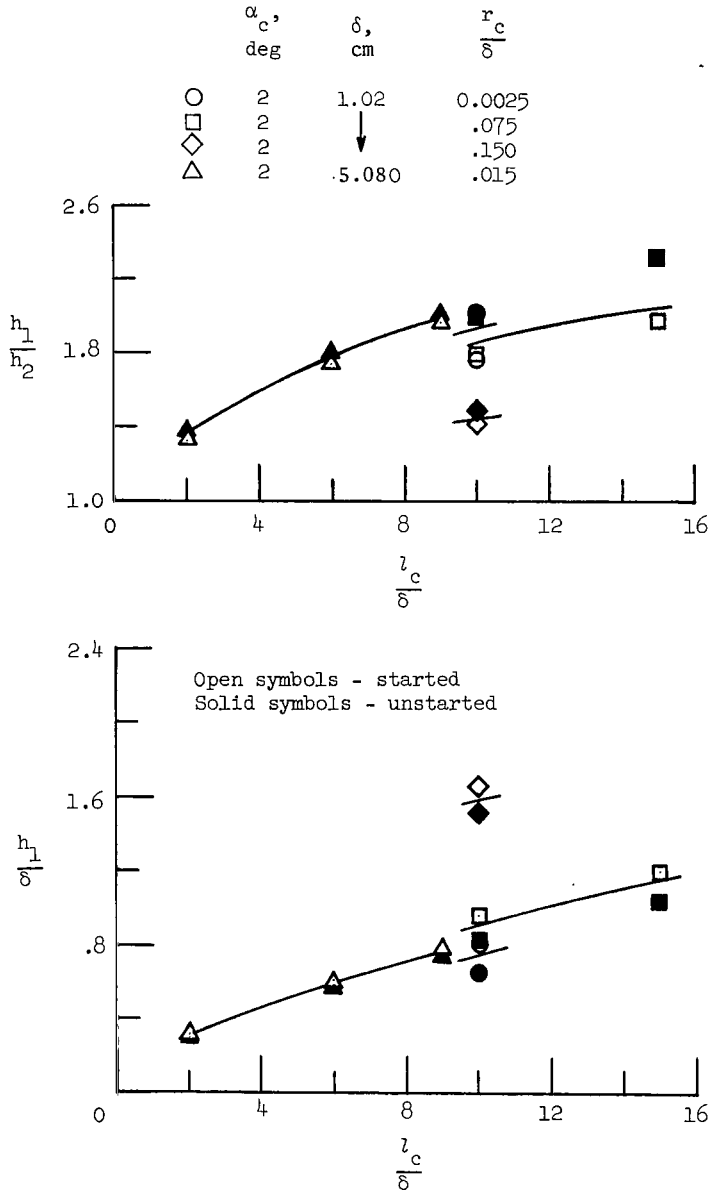

(c) Effect of cowl length.

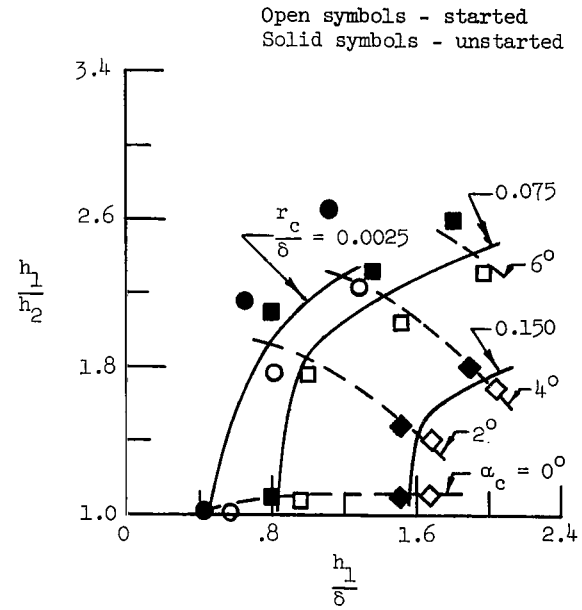

(d) Geometric effects. $l_c/\delta = 10$; $\delta = 1.02$ cm.

Figure 6.- Concluded.

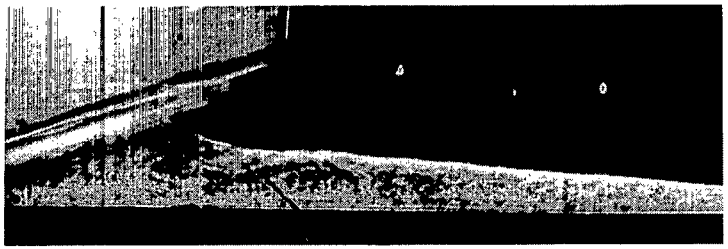

$h_1/\delta = 1.12$; $h_1/h_2 = 2.64$; unstarted

$h_1/\delta = 1.04$; $h_1/h_2 = 2.33$; unstarted

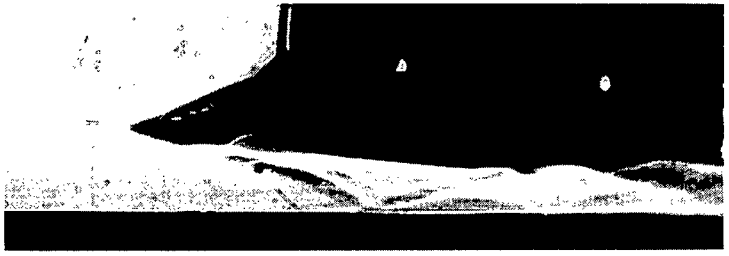

$h_1/\delta = 1.28$; $h_1/h_2 = 2.20$; started, no separation

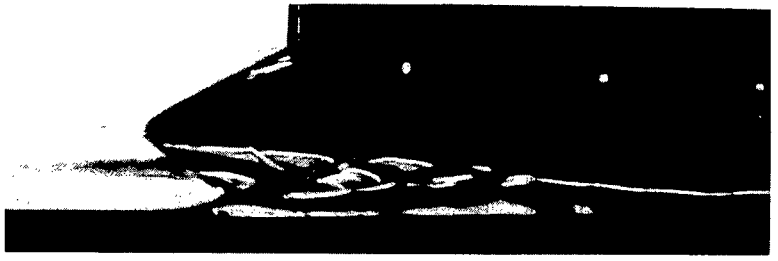

$h_1/\delta = 1.2$; $h_1/h_2 = 1.98$; started, separation

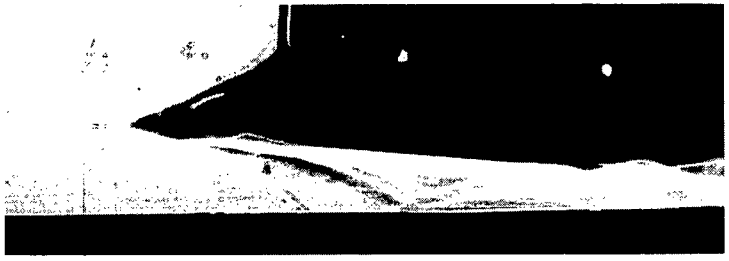

$h_1/\delta = 1.43$; $h_1/h_2 = 1.95$; started, no separation

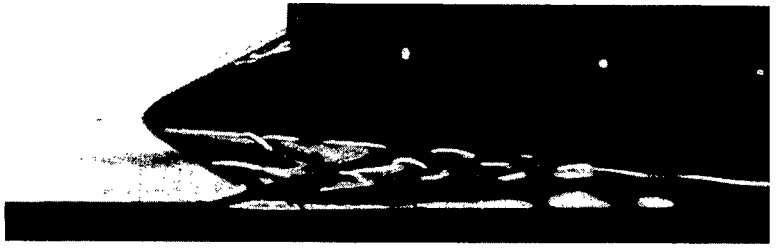

$h_1/\delta = 1.37$; $h_1/h_2 = 1.78$; started, separation

L-71-630

(a) $l_c/\delta = 10$; $r_c/\delta = 0.0025$; $\alpha_c = 4^o$.

(b) $l_c/\delta = 15$; $r_c/\delta = 0.075$; $\alpha_c = 2^o$.

Figure 7.- Schlieren photographs showing started and unstarted inlet configurations with and without separation. $\delta = 1.02$ cm; $R_\infty = 2.06 \times 10^7/m$.

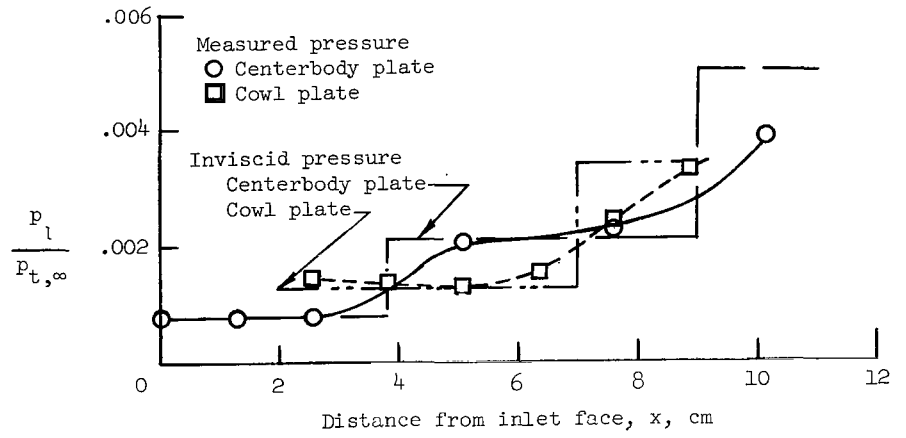

(a) Not separated; $l_c/\delta = 10$; $r_c/\delta = 0.0025$; $h_1/\delta = 1.28$; $h_1/h_2 = 1.95$; $\alpha_c = 4^o$.

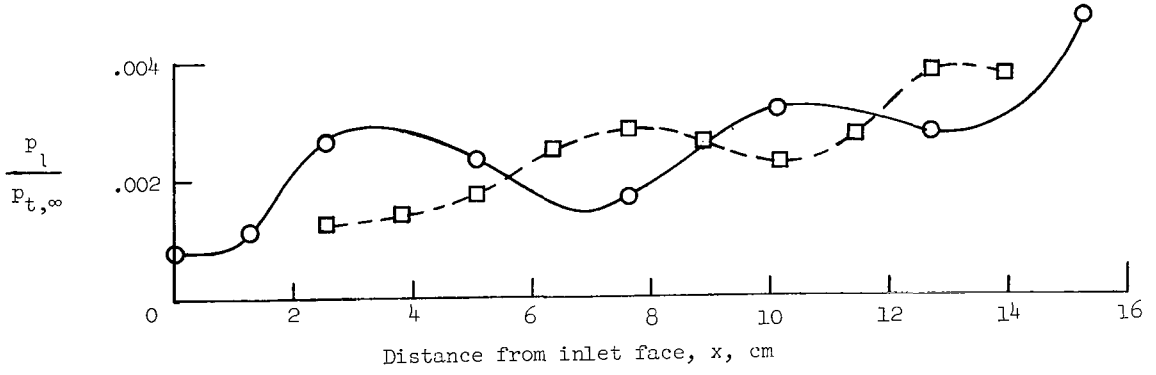

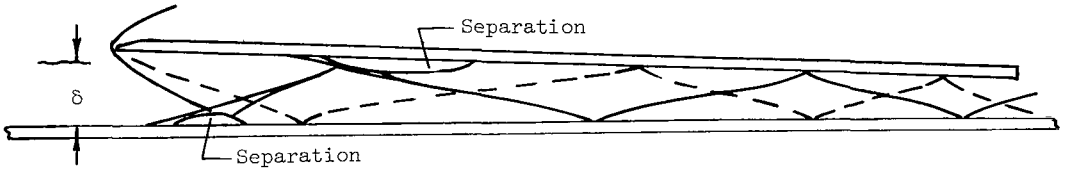

(b) Separated; $l_c/\delta = 15$; $r_c/\delta = 0.075$; $h_1/\delta = 1.37$; $h_1/h_2 = 1.78$; $\alpha_c = 2^o$.

Figure 8.- Typical static-pressure distributions and simplified flow patterns for started configurations with and without separation. $\delta = 1.02$ cm; $R_\infty = 2.06 \times 10^7$/m.

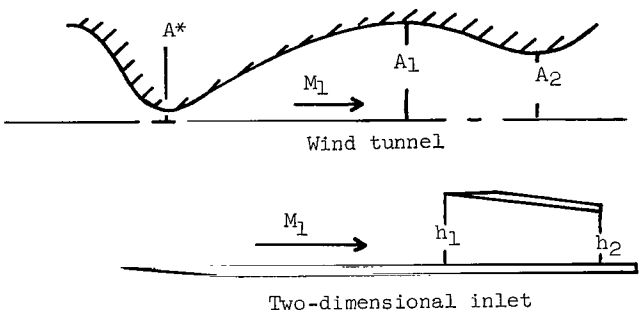

(a) Fixed-geometry configurations.

$$\frac{A_1}{A_2} = \frac{A_1}{A^*}\frac{P_{t,2}}{P_{t,1}}$$

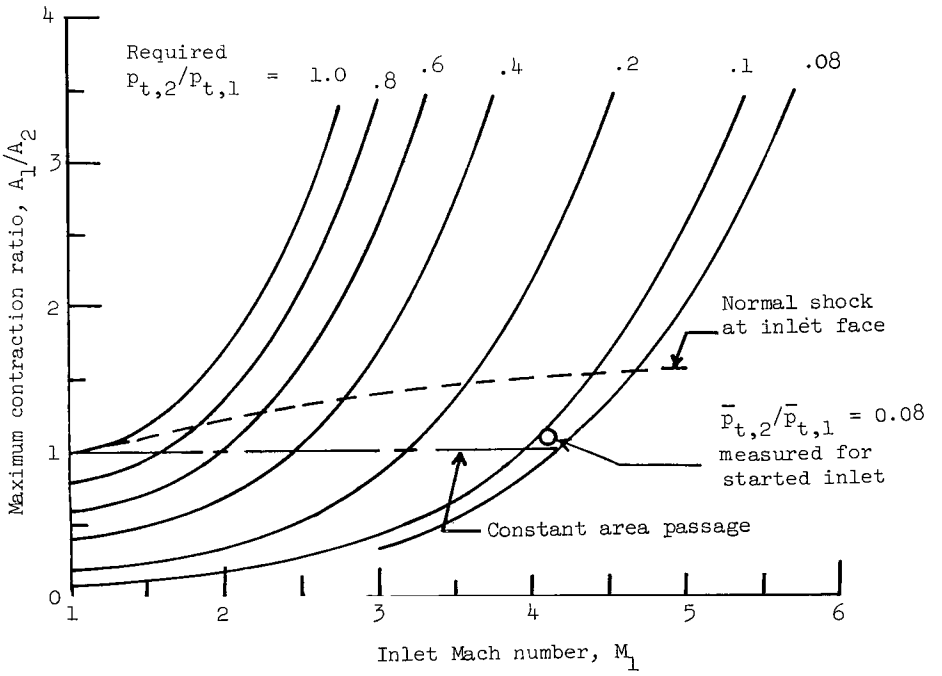

(b) Effect of total-pressure recovery.

Figure 9.- Starting parameters for hypersonic diffusers.

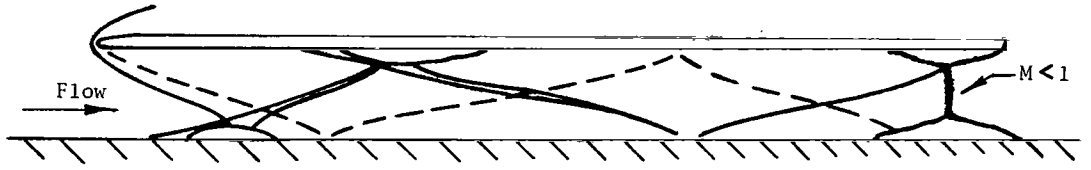

(a) Hypothetical unstarted condition.

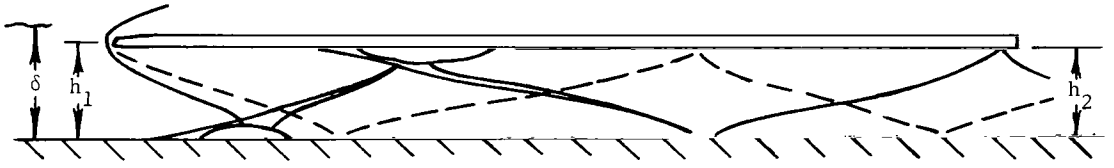

(b) Assumed started condition.

L-71-631

(c) Schlieren of typical started inlet.

Figure 10.- Flow patterns for hypersonic inlets with $h_1 \approx \delta$.

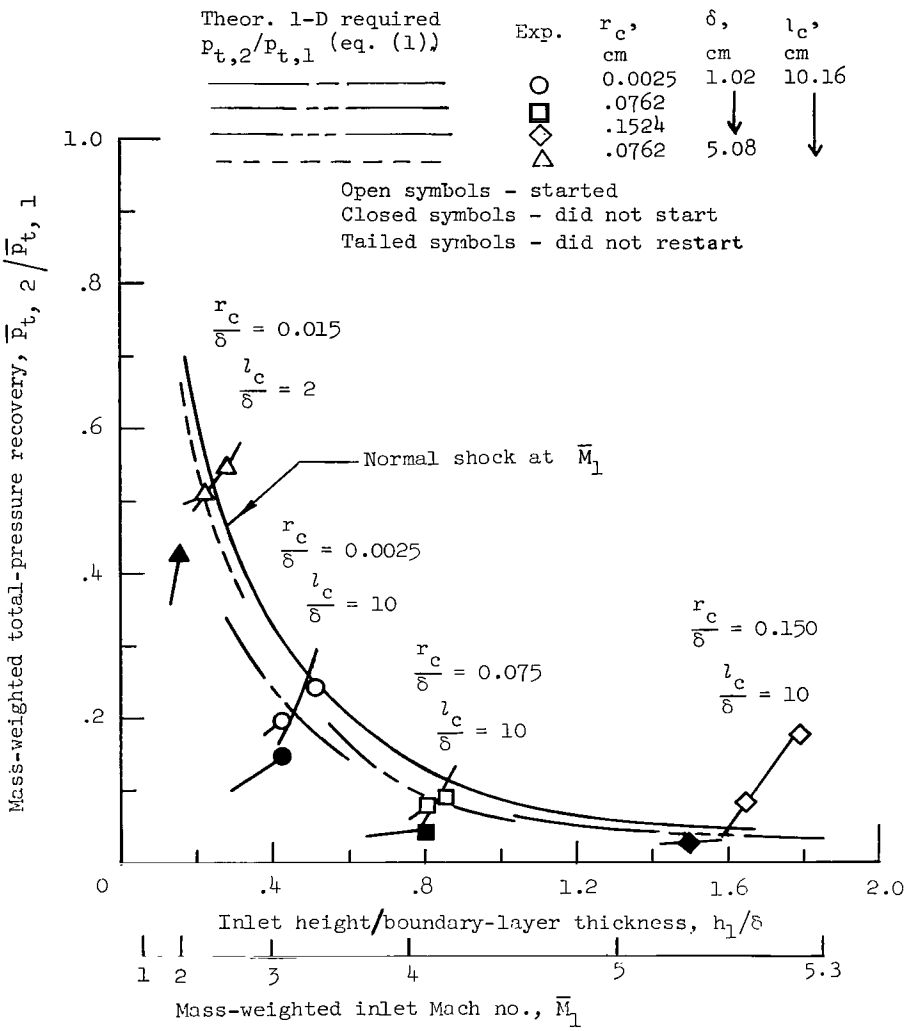

(a) $\alpha_c = 0^o$.

Figure 11.- Effect of total-pressure recovery on starting. $R_\infty = 2.06 \times 10^7$/m.

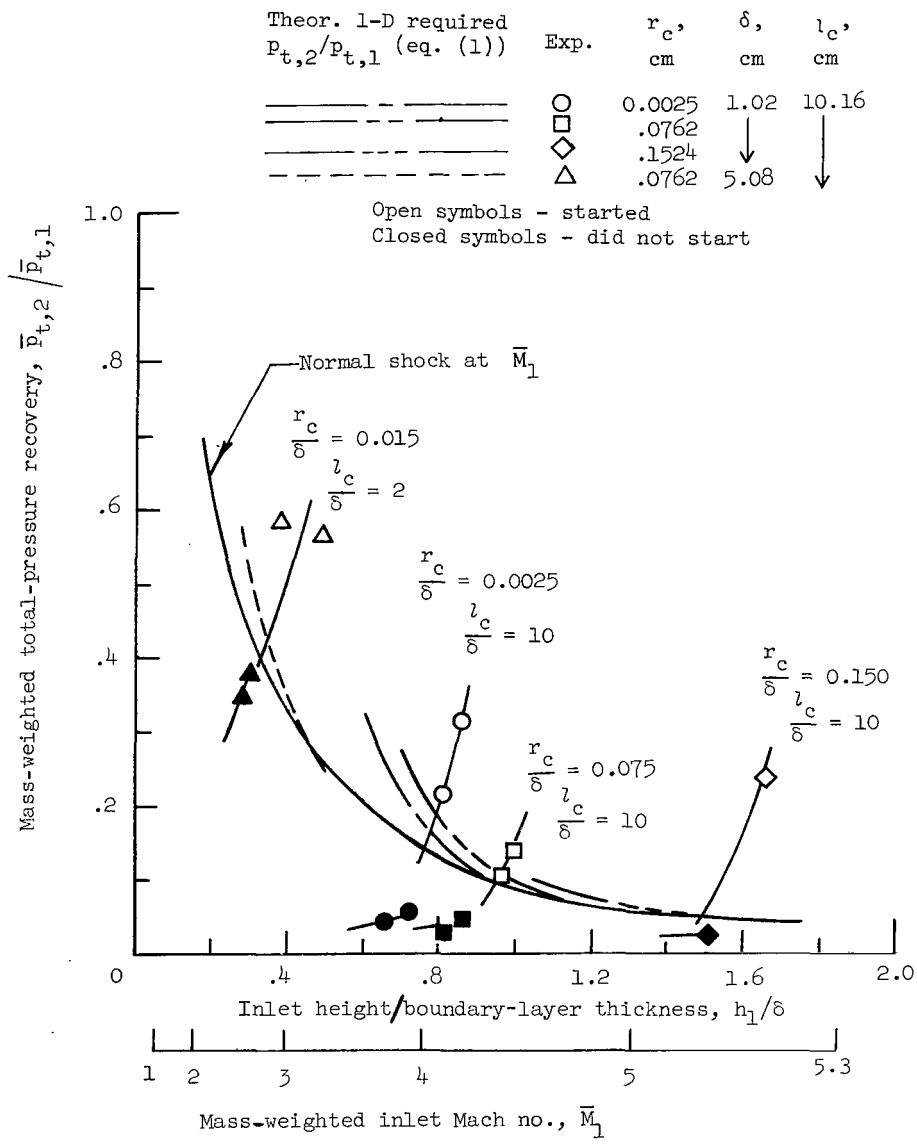

(b) $\alpha_c = 2^o$.

Figure 11.- Continued.

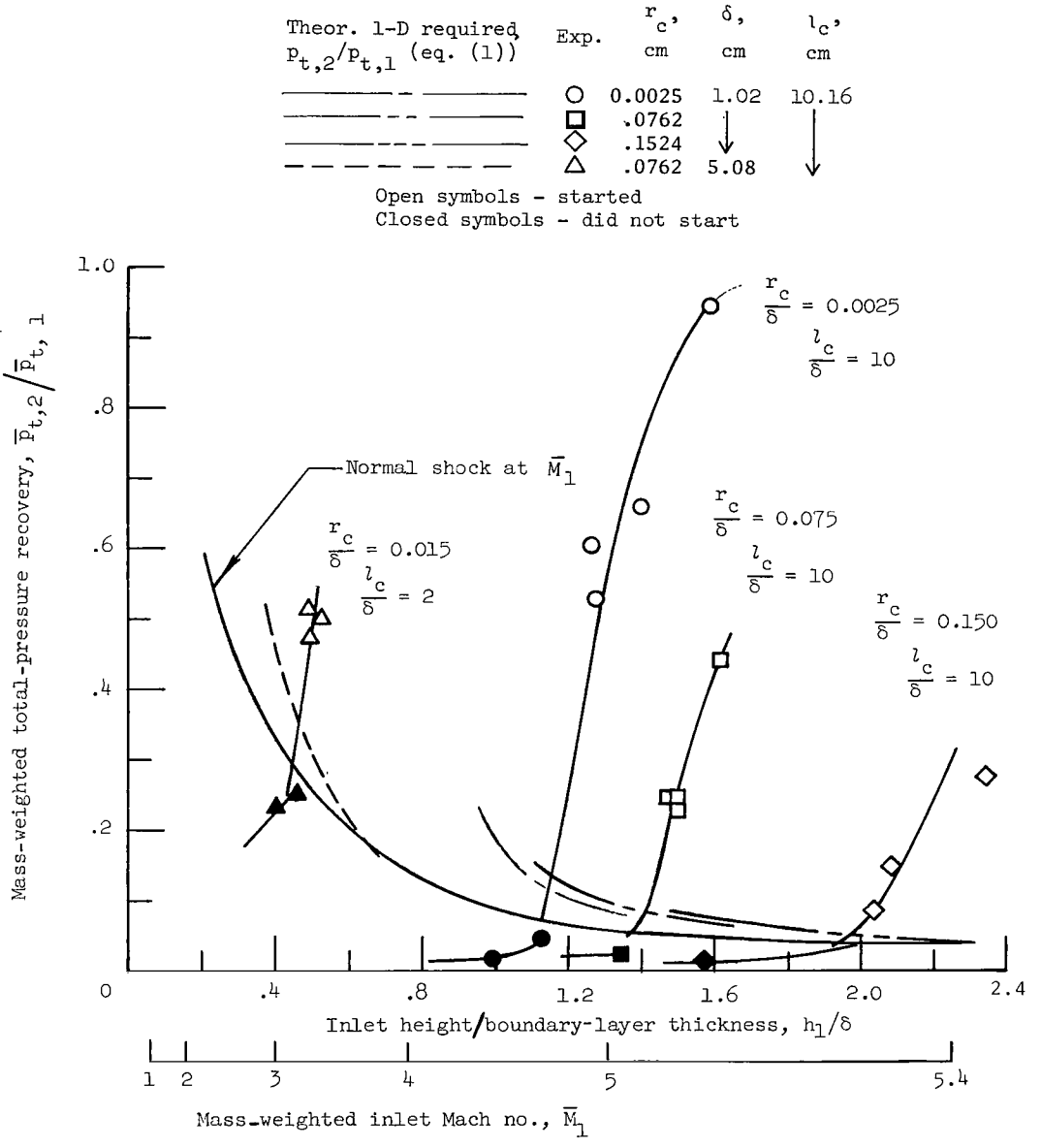

(c) $\alpha_c = 4^o$.

Figure 11.- Concluded.

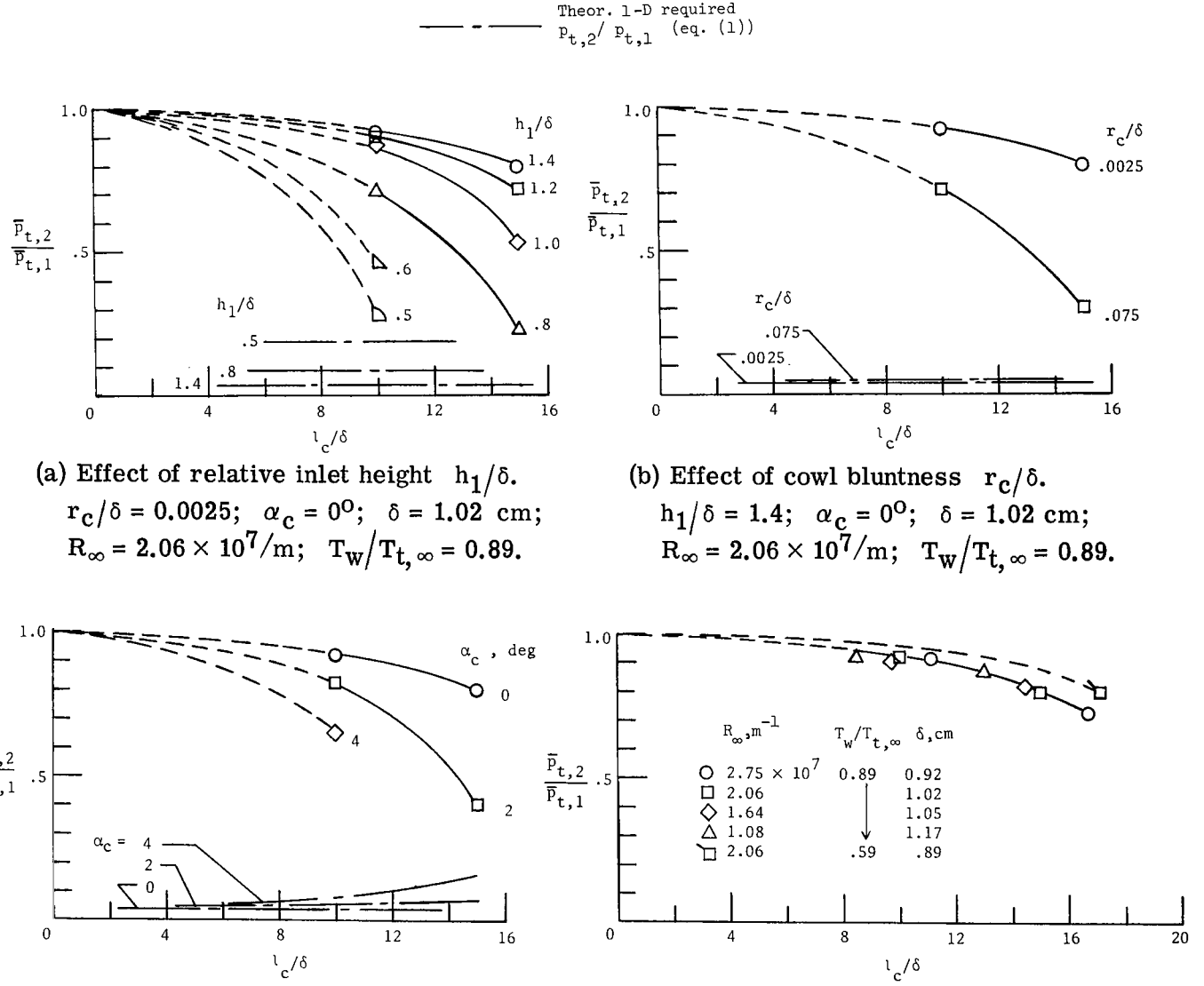

(a) Effect of relative inlet height h_1/δ. $r_c/\delta = 0.0025$; $\alpha_c = 0^o$; $\delta = 1.02$ cm; $R_\infty = 2.06 \times 10^7/m$; $T_w/T_{t,\infty} = 0.89$.

(b) Effect of cowl bluntness r_c/δ. $h_1/\delta = 1.4$; $\alpha_c = 0^o$; $\delta = 1.02$ cm; $R_\infty = 2.06 \times 10^7/m$; $T_w/T_{t,\infty} = 0.89$.

(c) Effect of cowl angle of attack α. $h_1/\delta = 1.4$; $r_c/\delta = 0.0025$; $\delta = 1.02$ cm; $R_\infty = 2.06 \times 10^7/m$; $T_w/T_{t,\infty} = 0.89$.

(d) Effect of free-stream Reynolds number R_∞/m. $h_1/\delta = 1.4$; $r_c = 0.00254$ cm.

Figure 12.- Effect of various parameters on inlet total-pressure recovery.

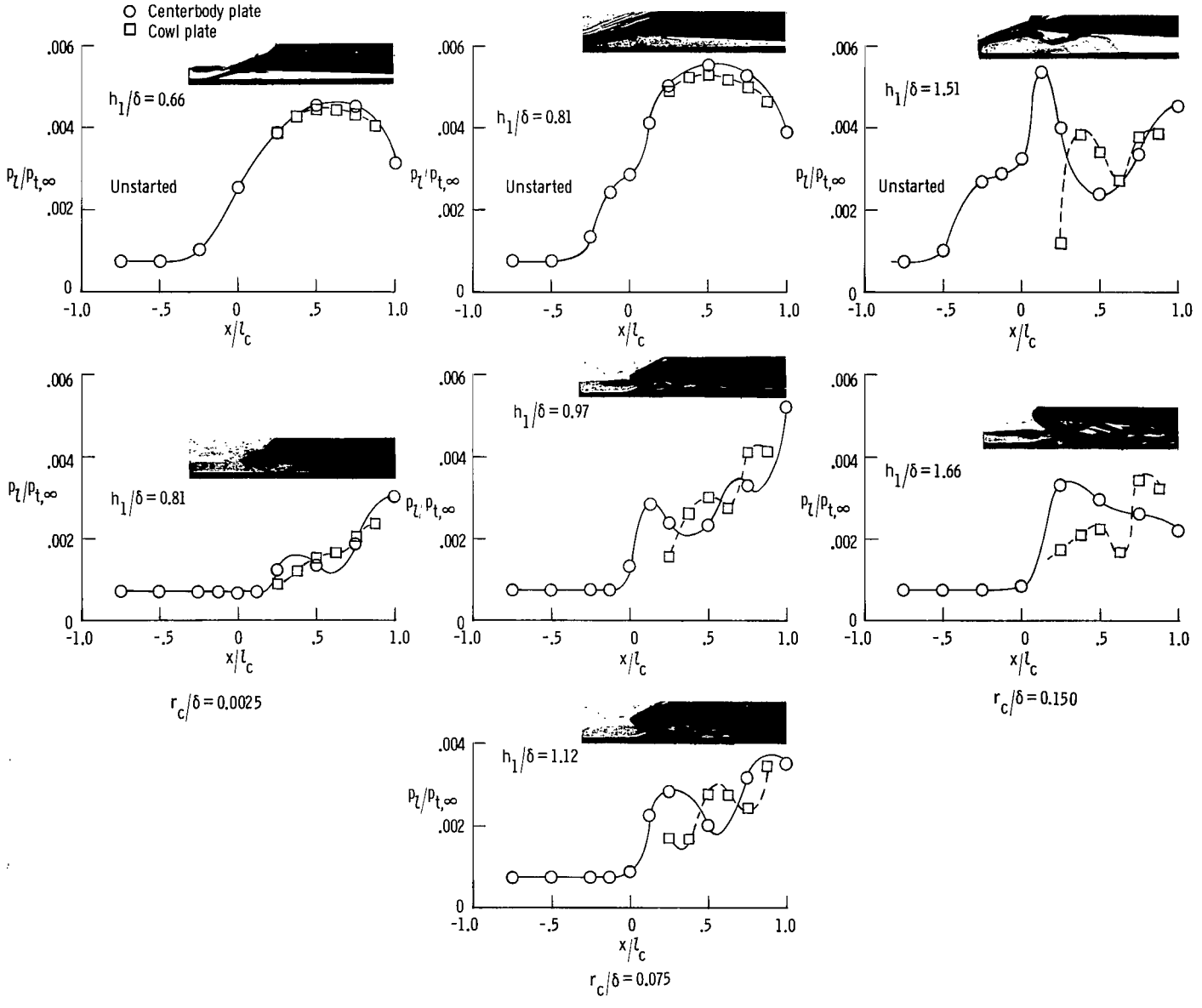

(a) Variation with cowl bluntness. $l_c/\delta = 10$; $\delta = 1.02$ cm; $\alpha_c = 2^o$.

Figure 13.- Static-pressure distributions. $R_\infty = 2.06 \times 10^7/m$.

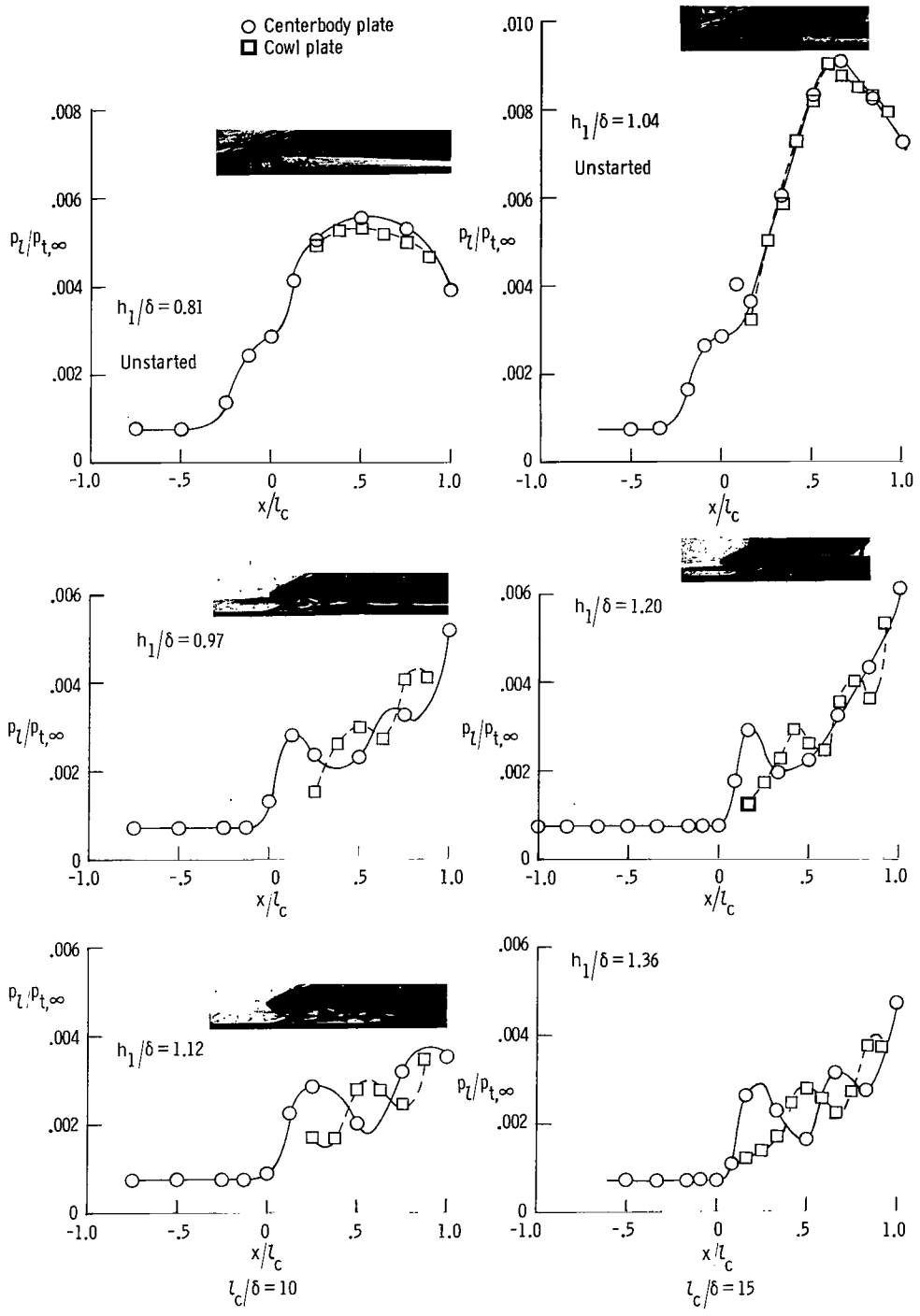

(b) Variation with cowl length. $r_c/\delta = 0.075$; $\delta = 1.02$ cm; $\alpha_c = 2^o$.

Figure 13.- Continued.

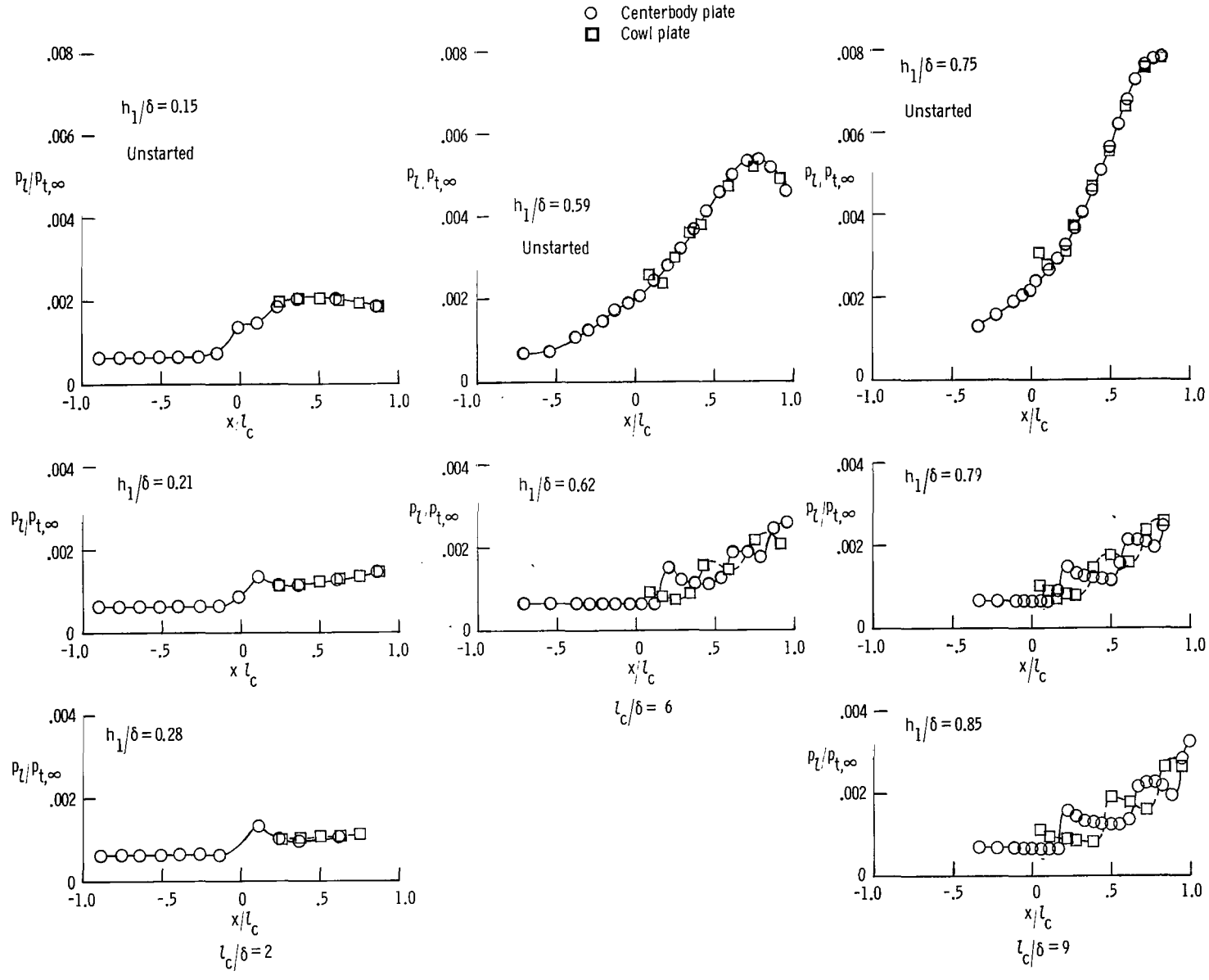

(c) Variation with cowl length. $r_c/\delta = 0.015$; $\delta = 5.08$ cm; $\alpha_c = 2^o$.

Figure 13.- Continued.

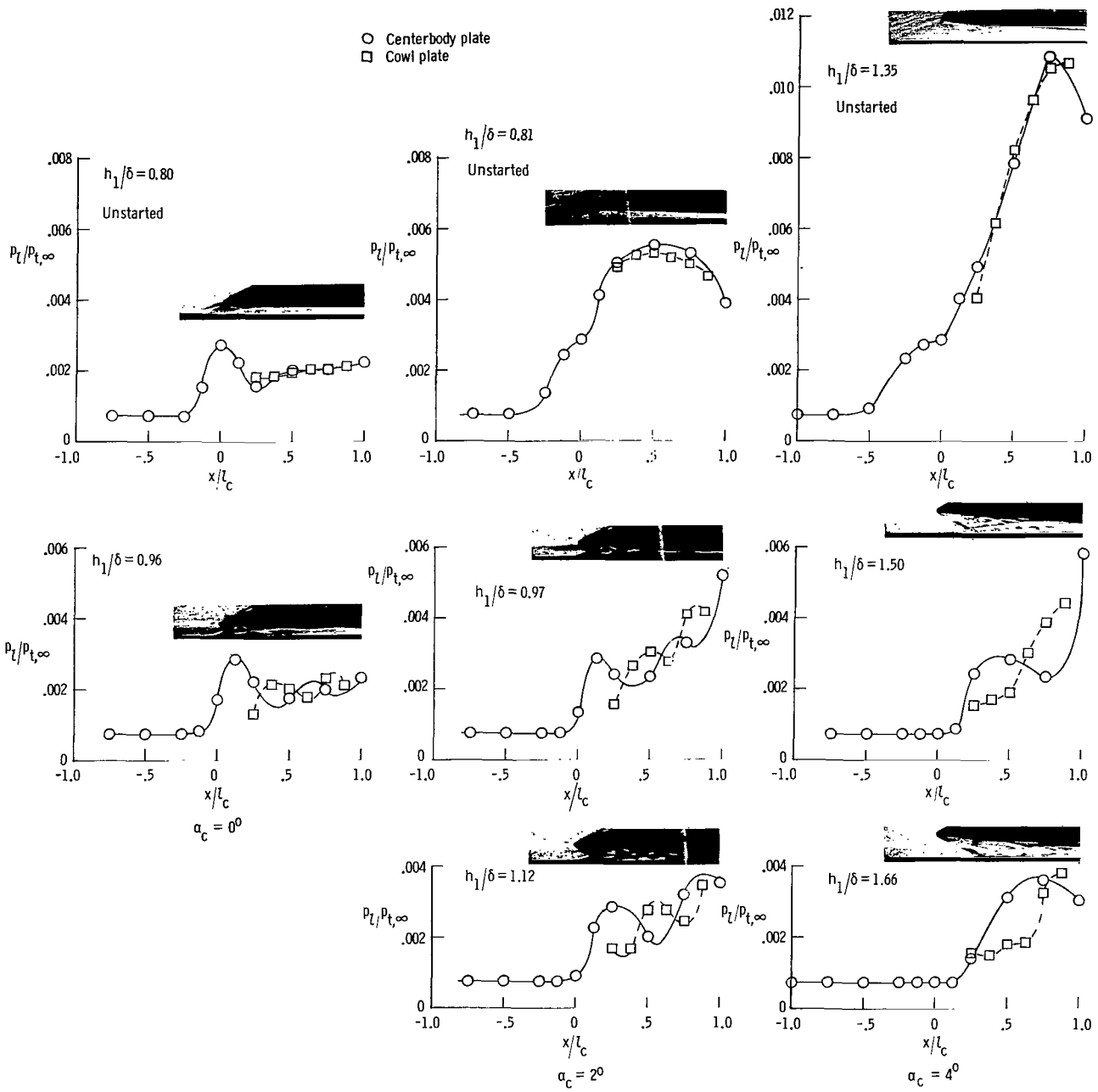

(d) Variation with cowl angle of attack. $r_c/\delta = 0.075$; $l_c/\delta = 10$; $\delta = 1.02$ cm.

Figure 13.- Continued.

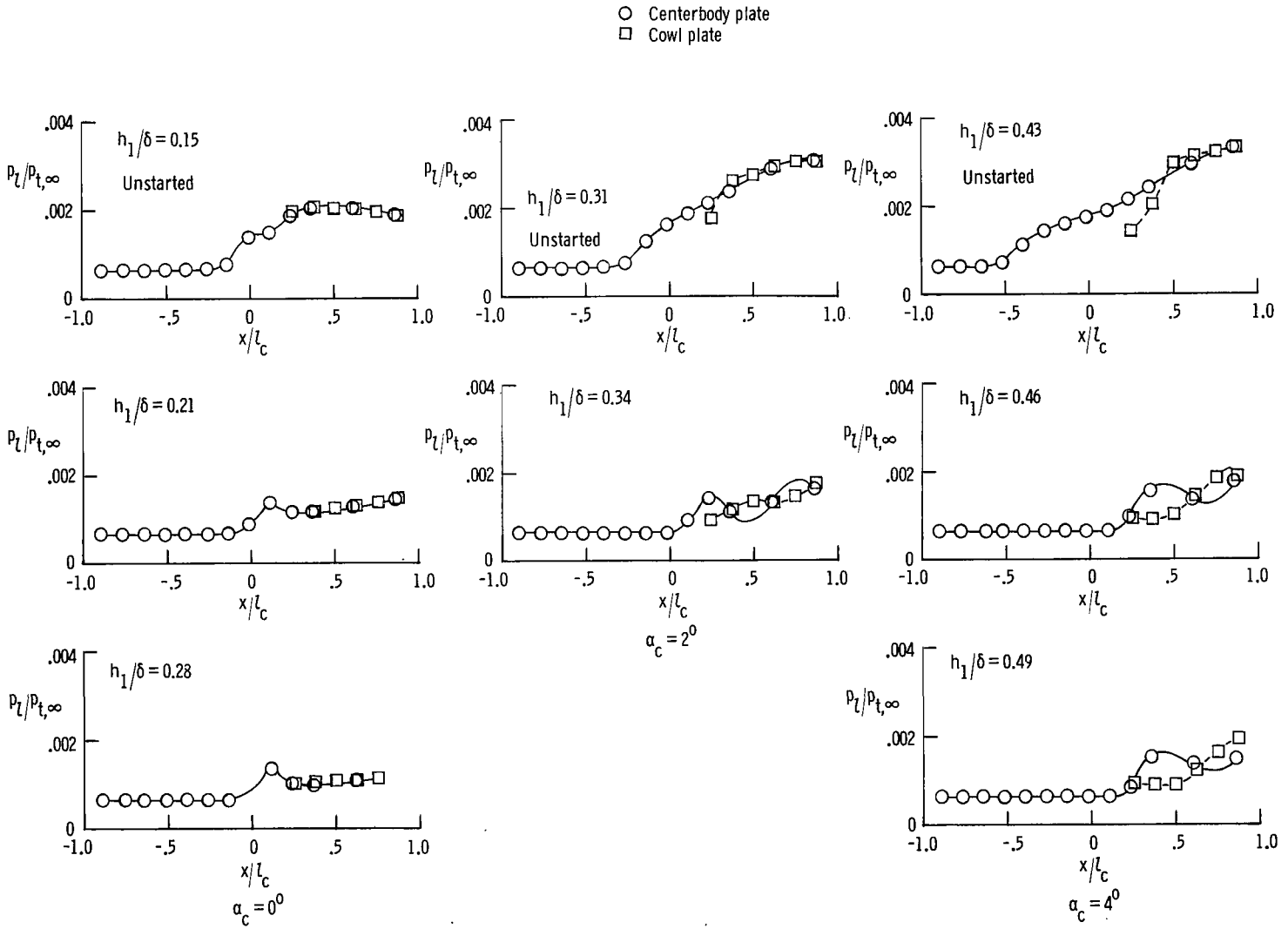

(e) Variation with cowl angle of attack. $l_c/\delta = 2.0$; $r_c/\delta = 0.015$; $\delta = 5.08$ cm.

Figure 13.- Continued.

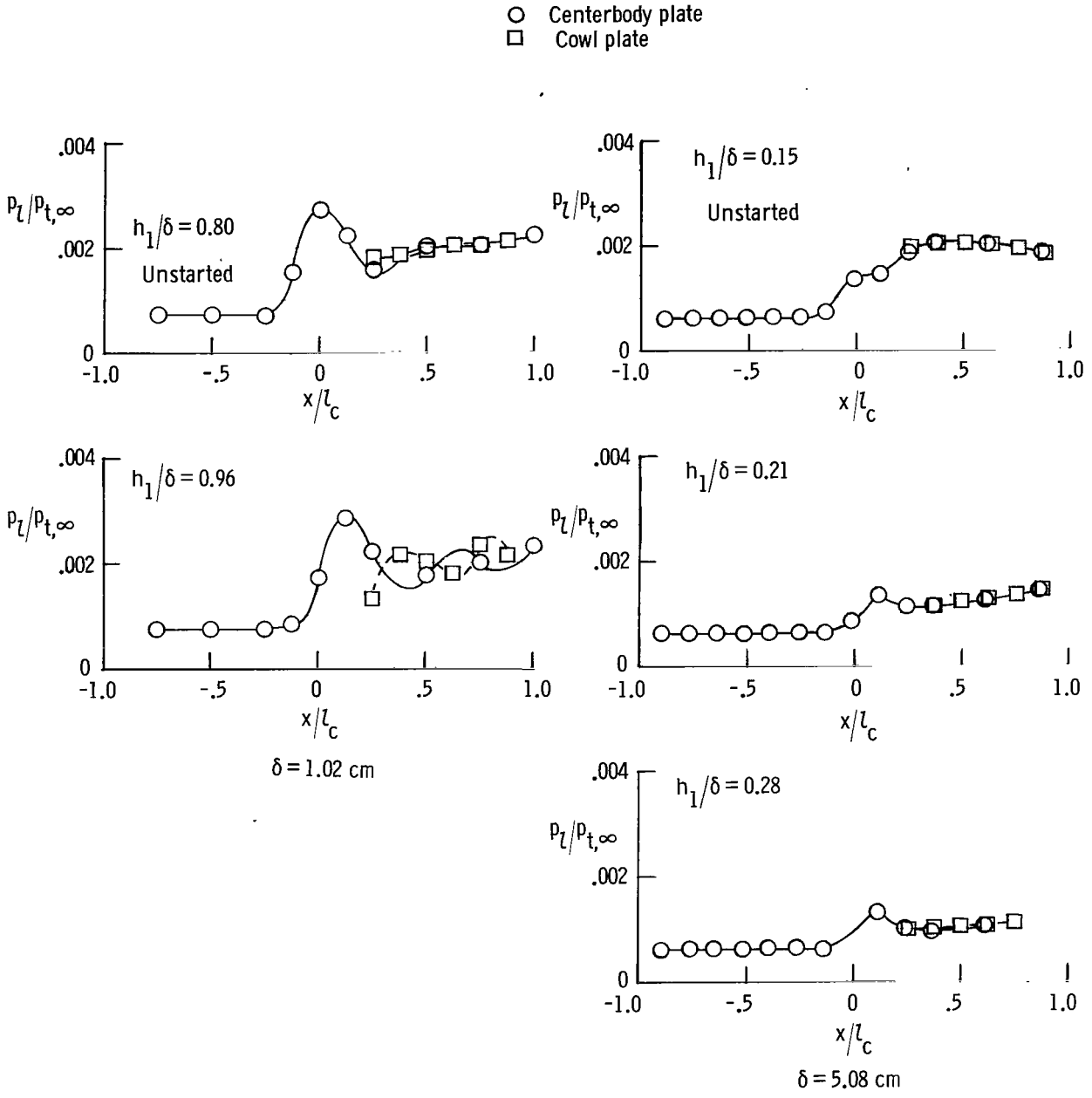

(f) Variation with boundary-layer thickness. l_c = 10.16 cm; r_c = 0.0762 cm; $\alpha_c = 0^o$.

Figure 13.- Concluded.

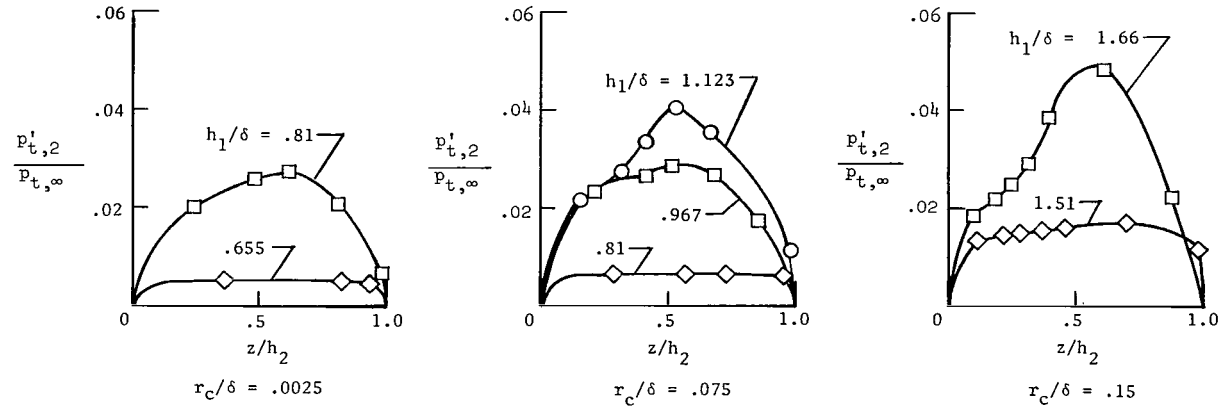

(a) Variation with cowl bluntness. $l_c/\delta = 10$; $\alpha_c = 2^o$; $\delta = 1.02$ cm.

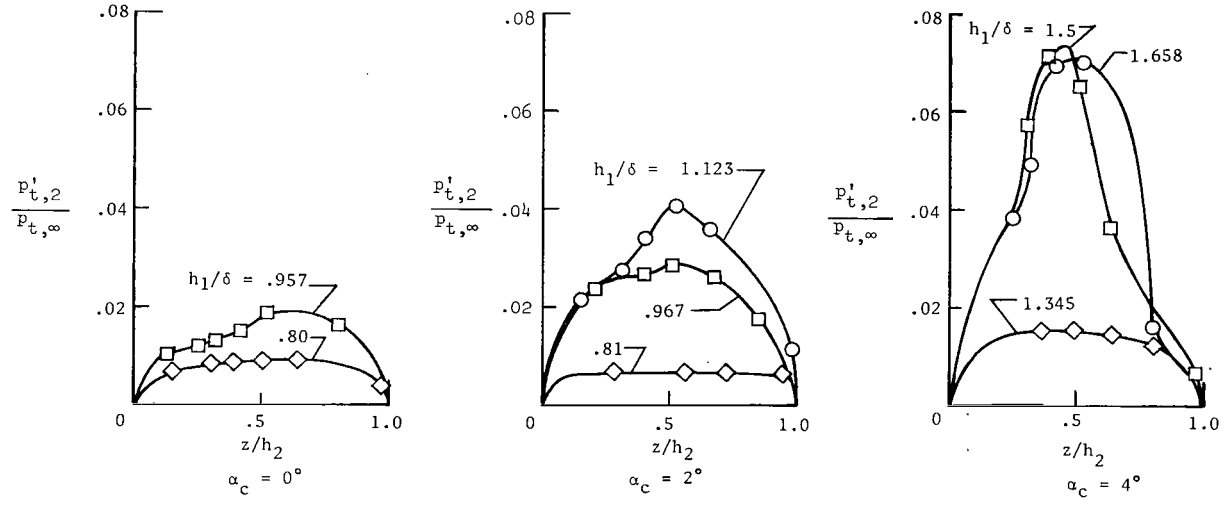

(b) Variation with cowl angle of attack. $r_c/\delta = 0.075$; $l_c/\delta = 10$; $\delta = 1.02$ cm.

(c) Variation with cowl angle of attack. $r_c/\delta = 0.015$; $l_c/\delta = 2$; $\delta = 5.08$ cm.

Figure 14.- Pitot-pressure profiles at exit station. $R_\infty = 2.06 \times 10^7/m$.

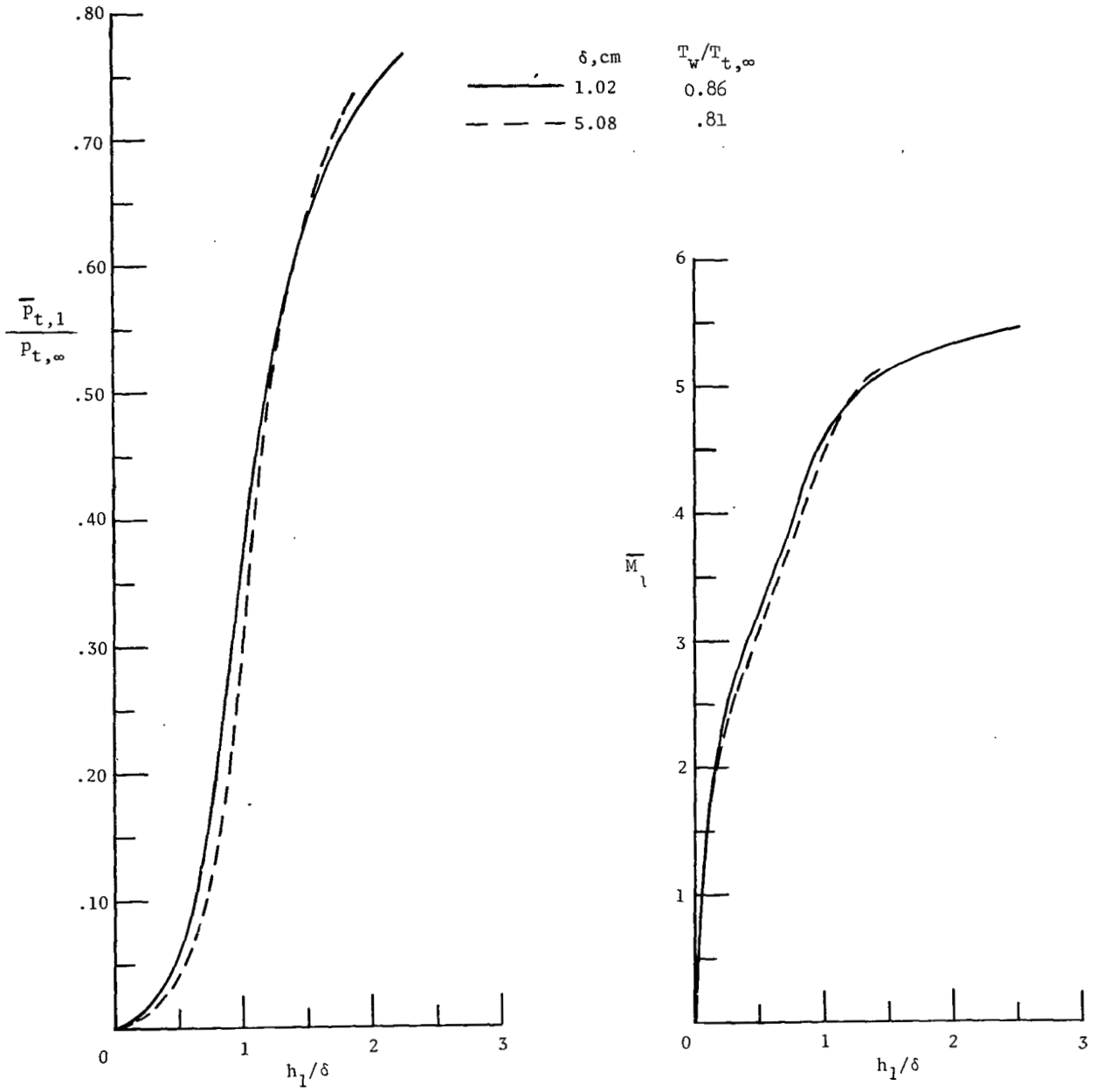

Figure 15.- Mass-weighted inlet total pressure and Mach number. $R_\infty = 2.06 \times 10^7/m$.

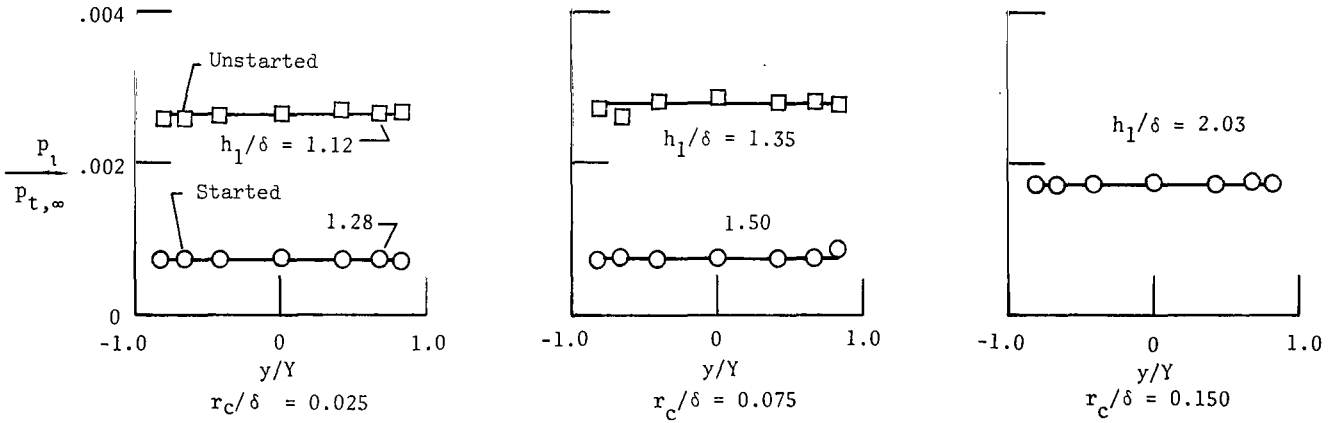

(a) $l_c/\delta = 10$; $x/l_c = 0$; $\delta = 1.02$ cm; $\alpha_c = 4^o$.

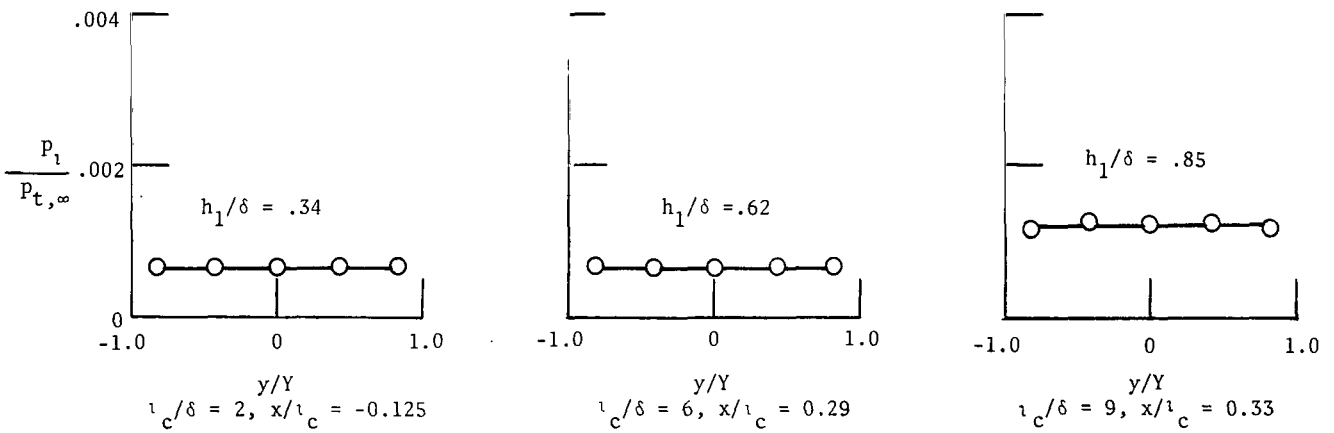

(b) $r_c/\delta = 0.015$; $\delta = 5.08$ cm; $\alpha_c = 2^o$.

Figure 16.- Typical spanwise pressure distributions on centerbody plate. $R_\infty = 2.06 \times 10^7/m$.

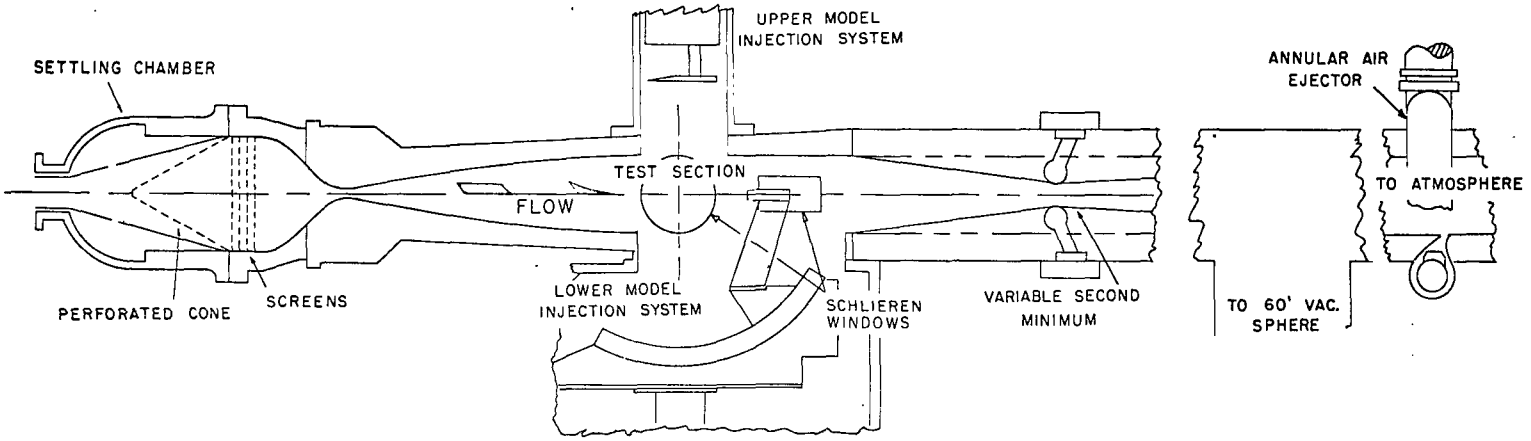

Figure A1.- Langley 20-inch Mach 6 tunnel.

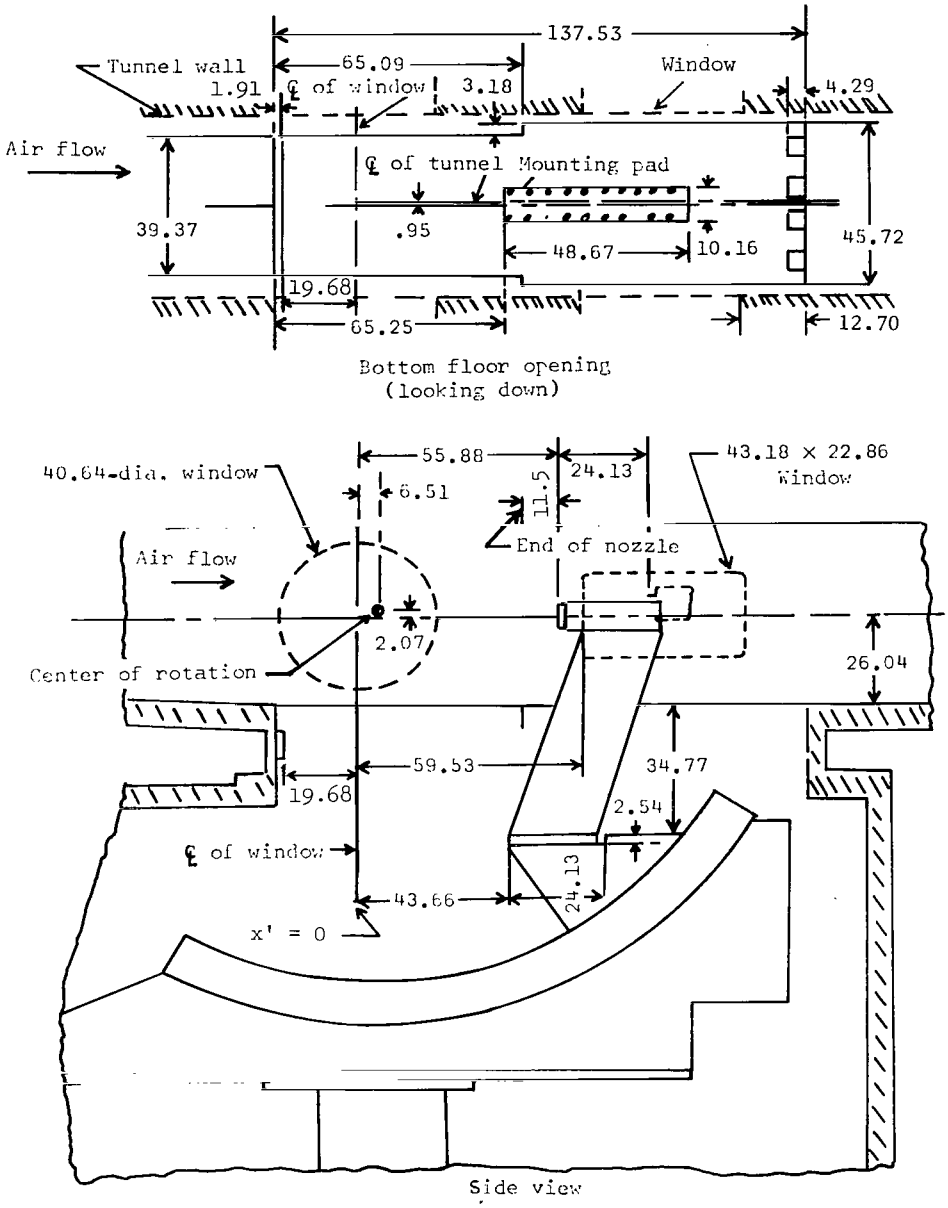

Figure A2.- Lower model injection system for Langley 20-inch Mach 6 tunnel. All dimensions are in cm.

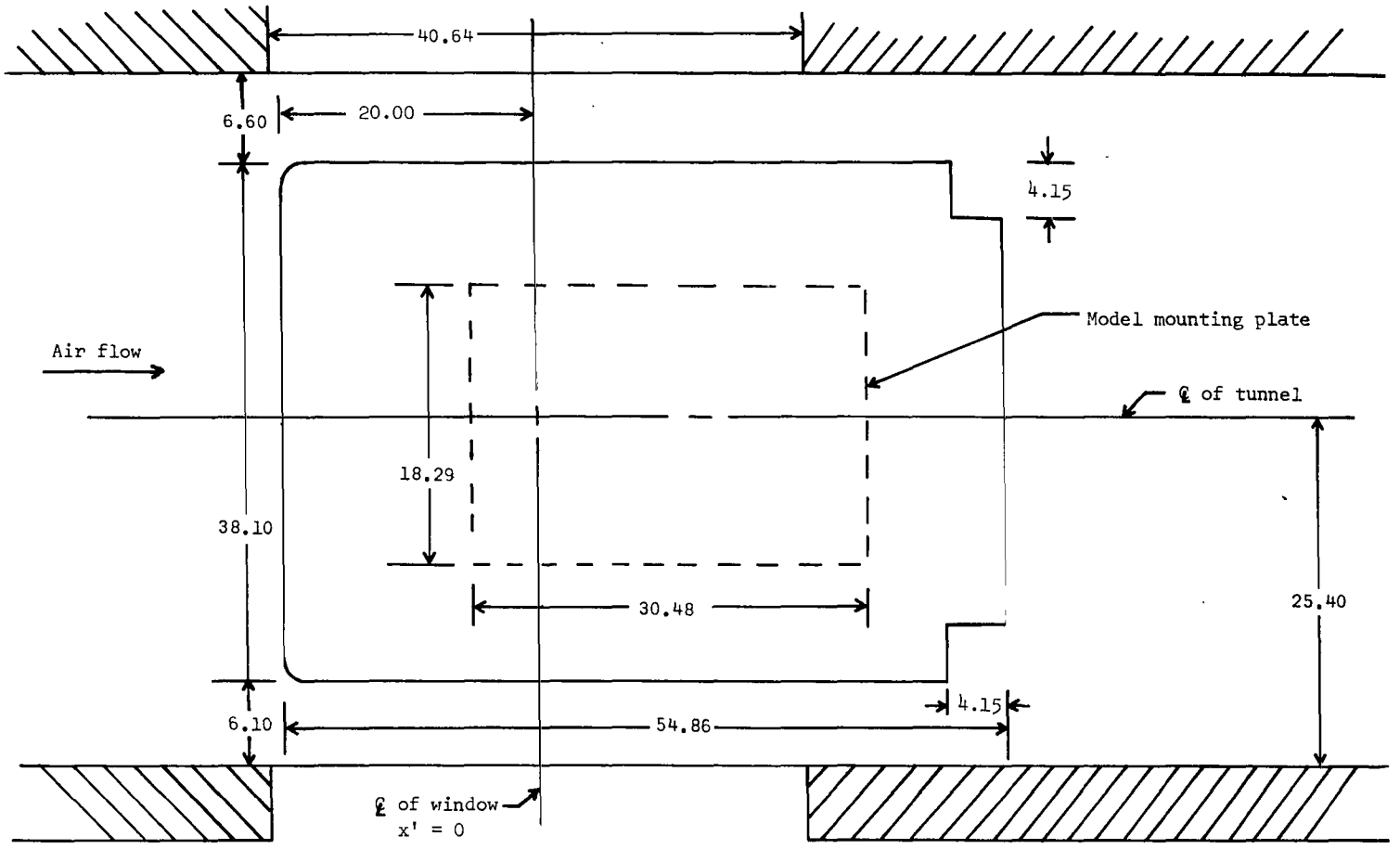

Figure A3.- Top injection-system opening for Langley 20-inch Mach 6 tunnel. All dimensions are in cm.

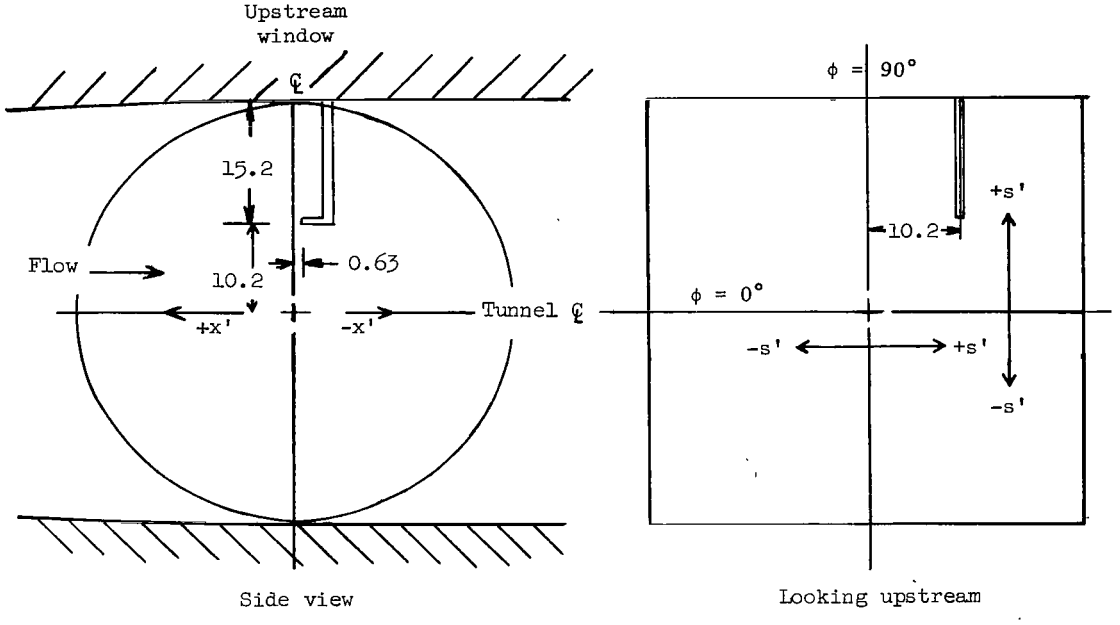

Figure A4.- Probe location. All dimensions are in cm.

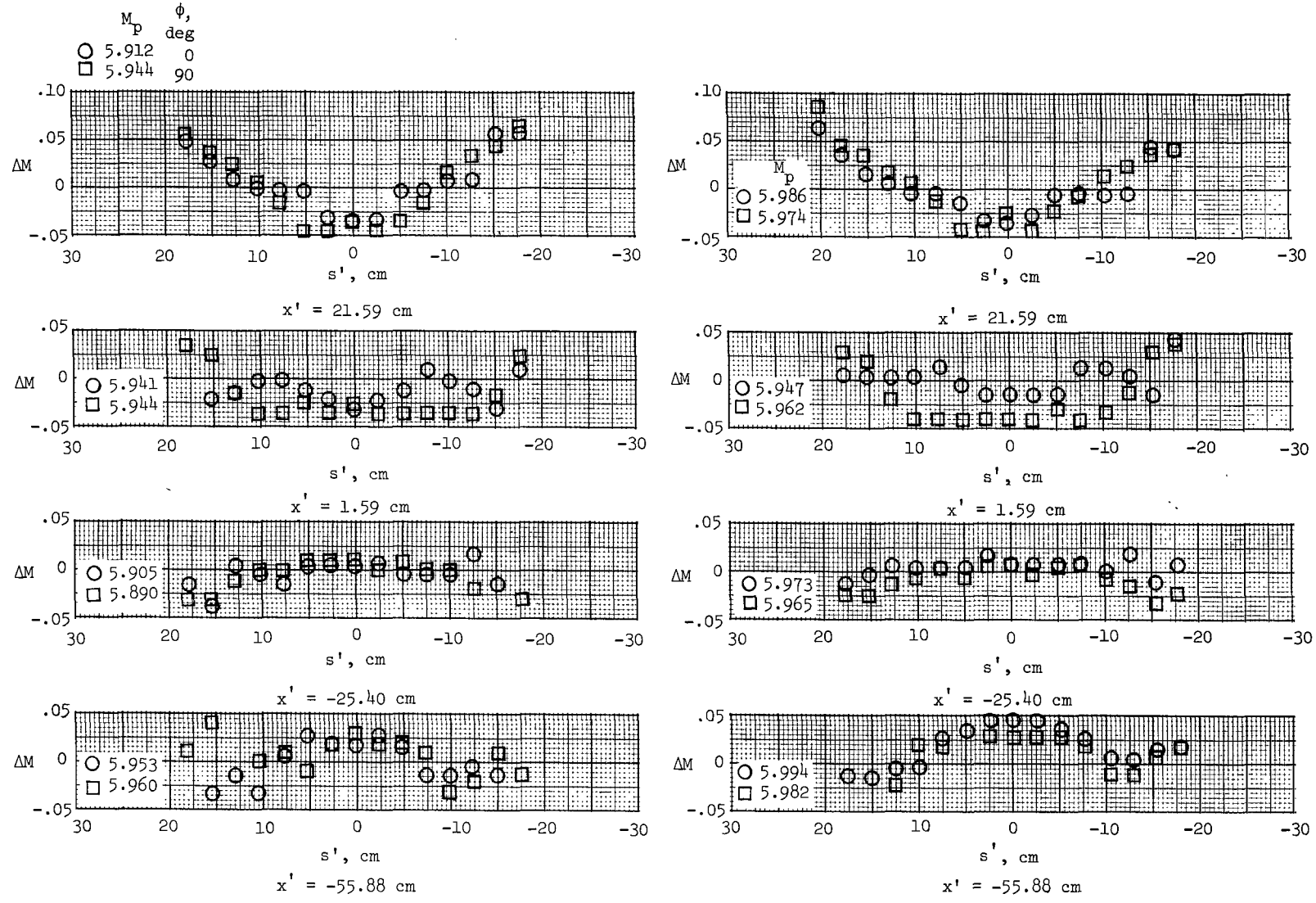

(a) $p_{t,1} = 0.52$ MN/m^2.

(b) $p_{t,1} = 1.14$ MN/m^2.

Figure A5.- Mach number deviation as a function of span.

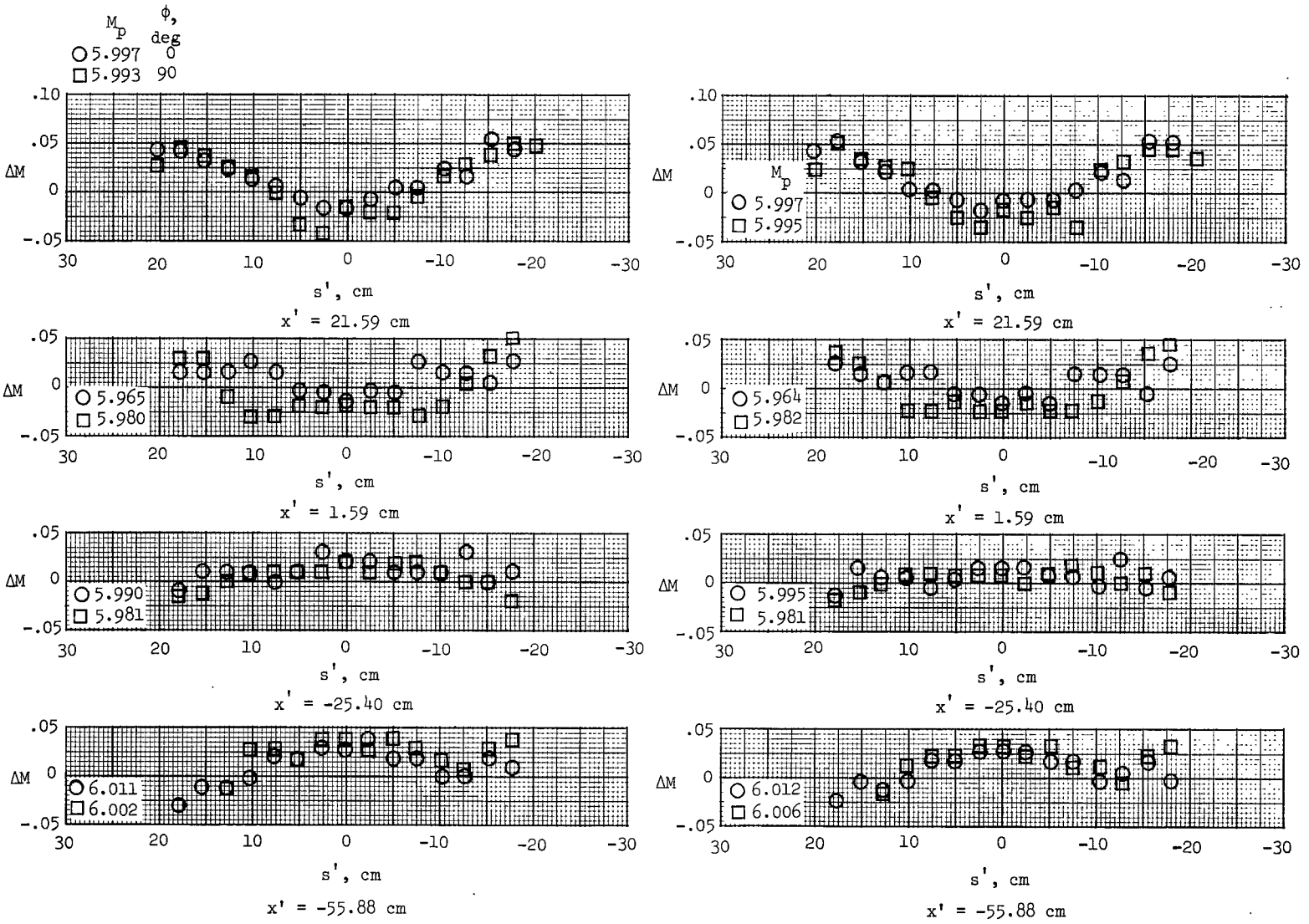

(c) $p_{t,1} = 2.17$ MN/m^2.

(d) $p_{t,1} = 3.03$ MN/m^2.

Figure A5.- Concluded.

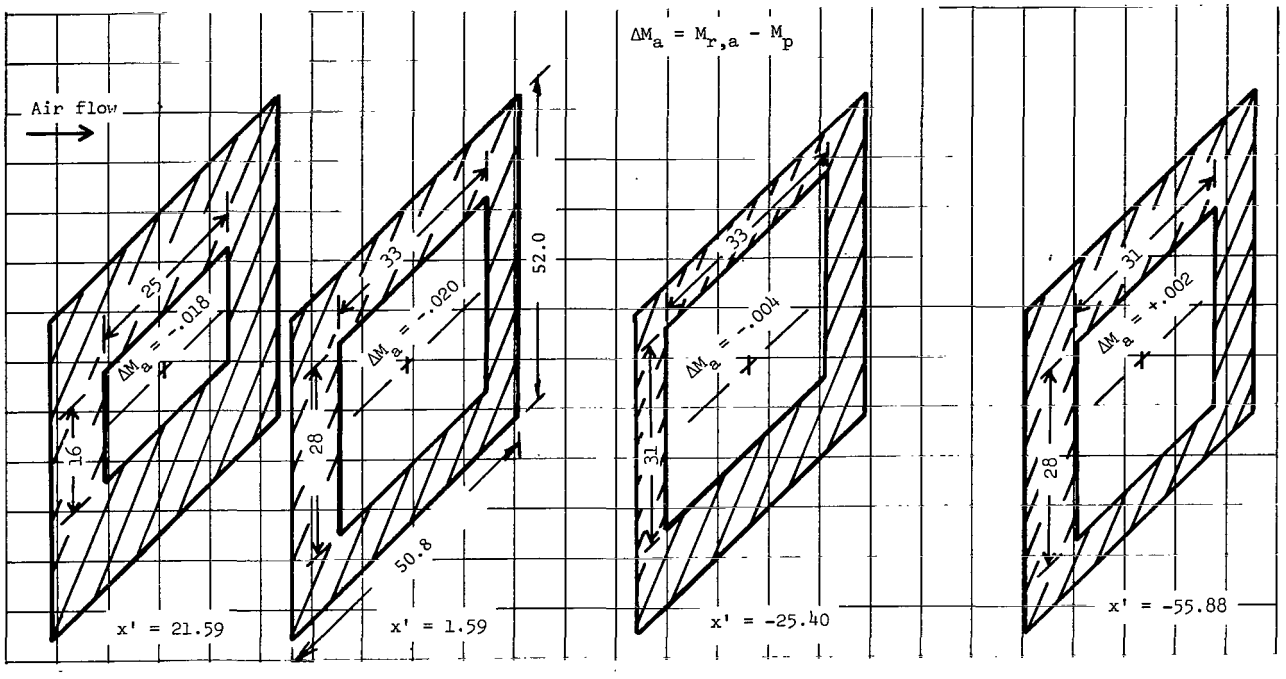

(a) $p_{t,1} = 0.52$ MN/m^2.

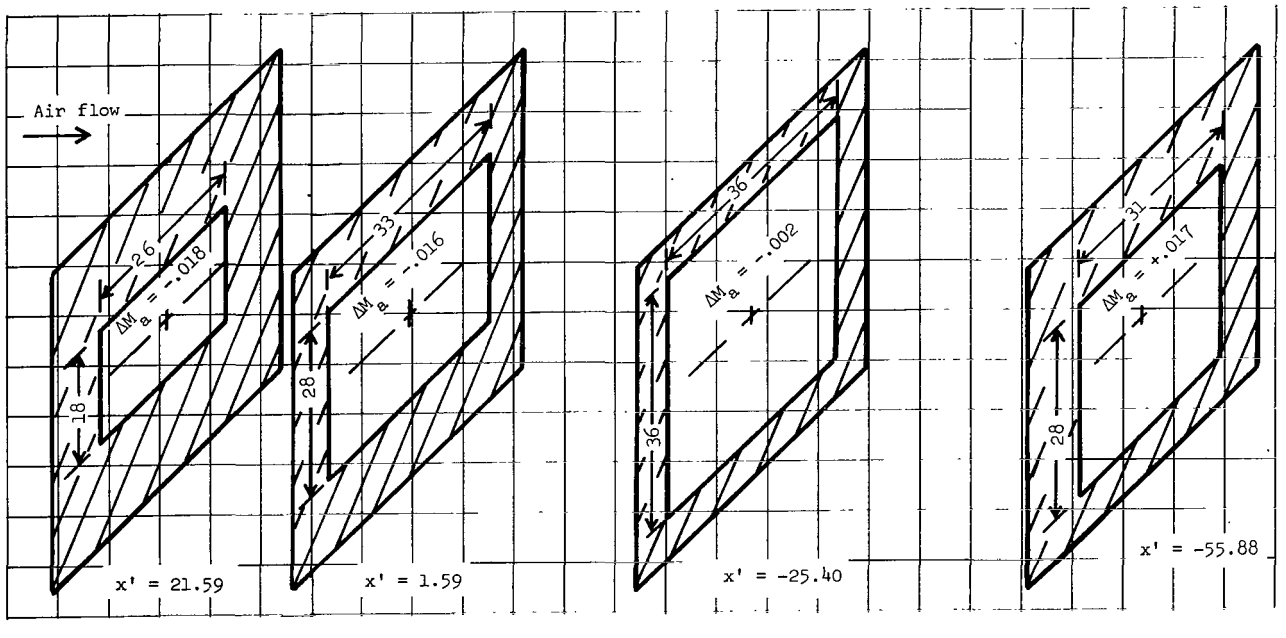

(b) $p_{t,1} = 1.14$ MN/m^2.

Figure A6.- Flow window at various axial stations. All dimensions are in cm.

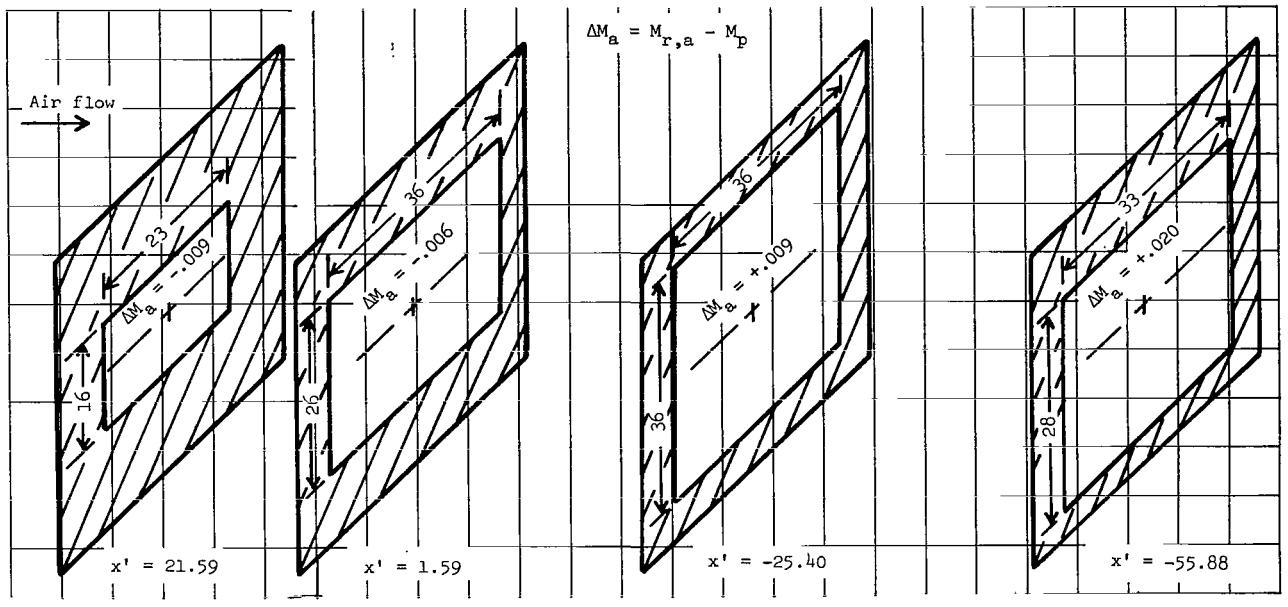

(c) $p_{t,1} = 2.17$ MN/m^2.

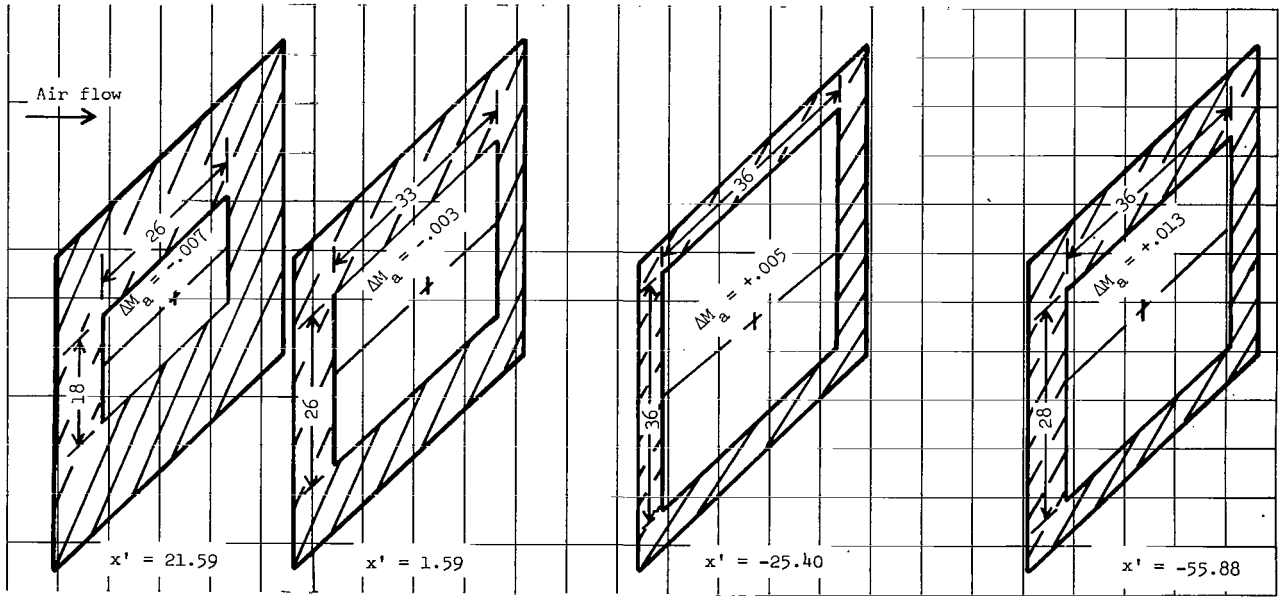

(d) $p_{t,1} = 3.03$ MN/m^2.

Figure A6.- Concluded.

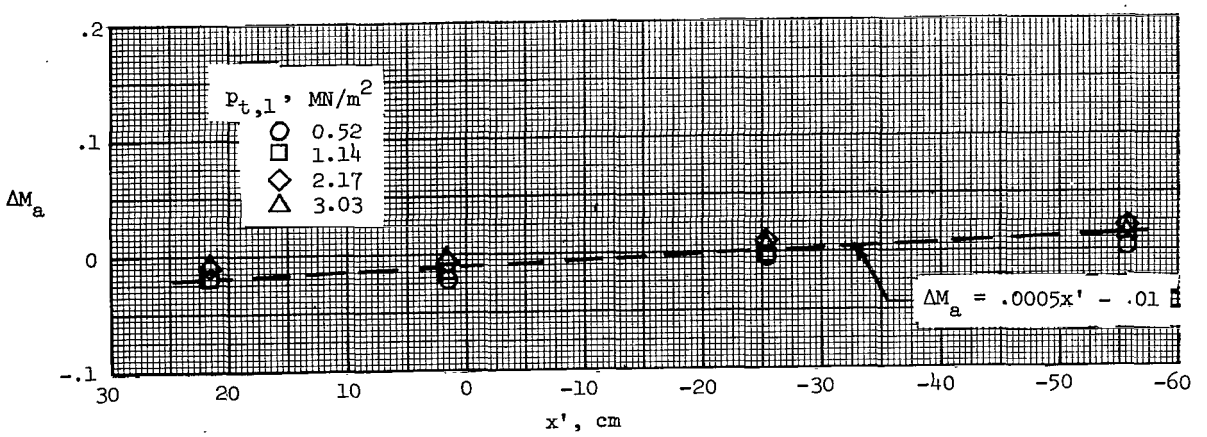

Figure A7.- Variation of ΔM_a with x'.

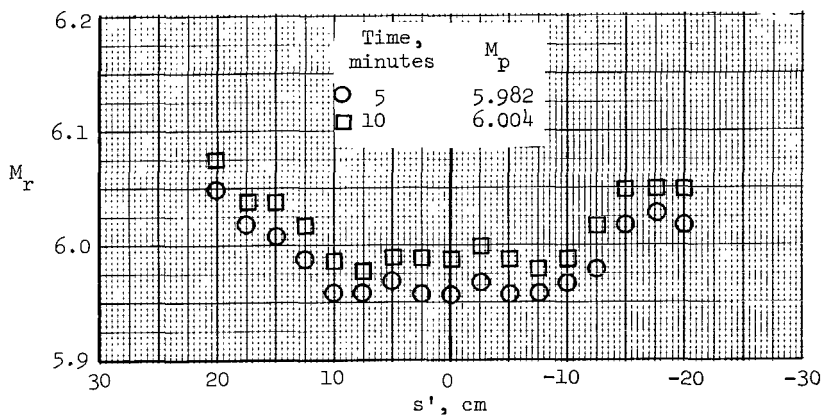

(a) Rake Mach number distribution with no adjustment.

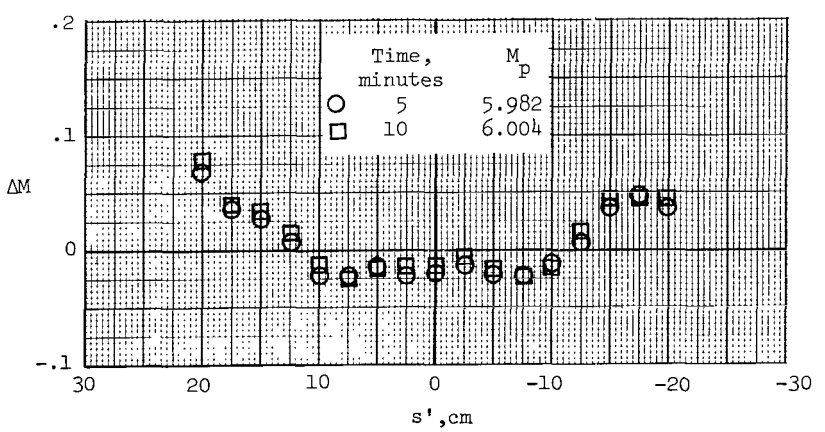

(b) Differential Mach number distribution.

Figure A8.- Mach number variation with time. x' = 1.59 cm; $\phi = 90^o$; $p_{t,1} = 3.03$ MN/m^2.

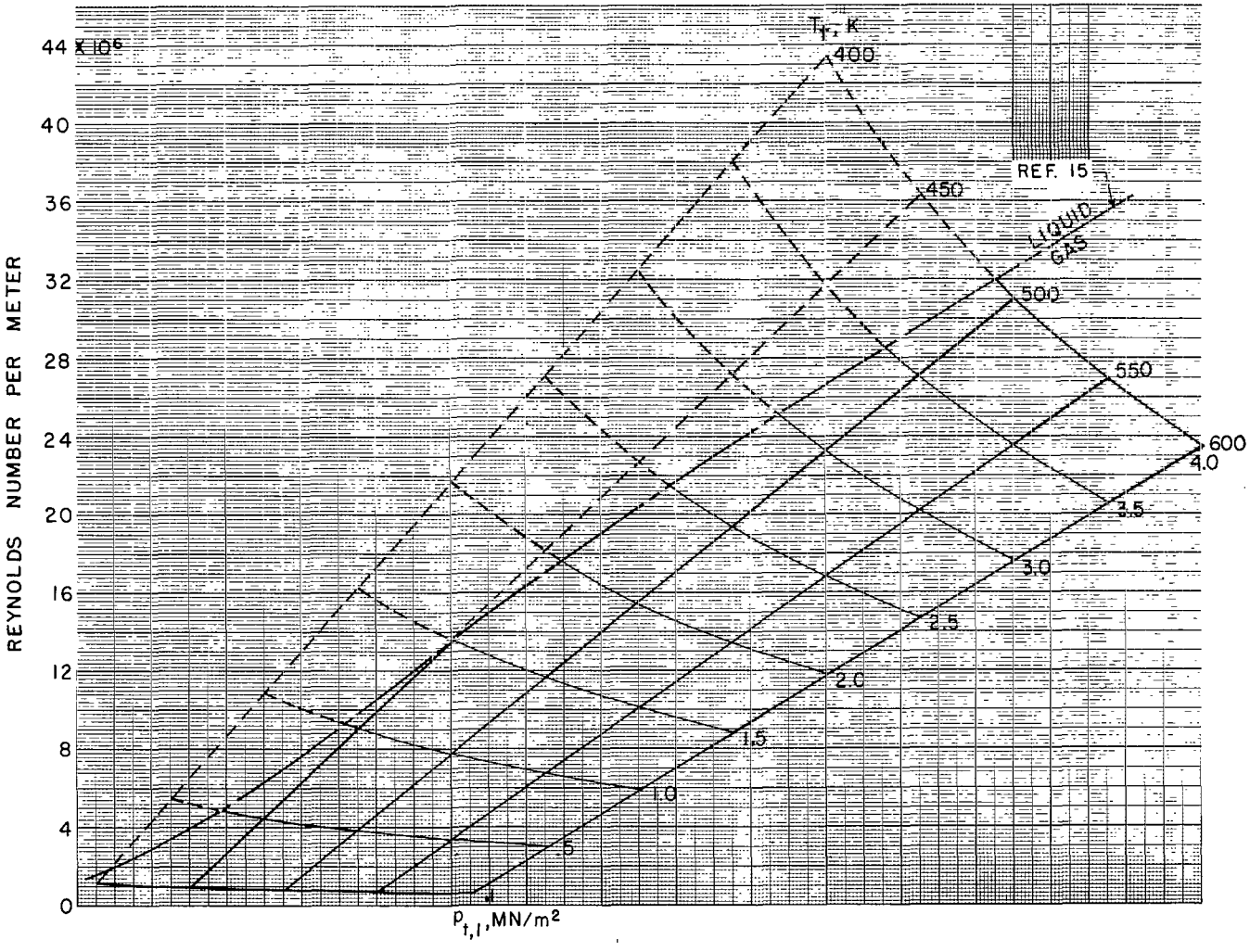

Figure A9.- Reynolds number as a function of stagnation pressure and temperature for M = 6. $\mu = 398.36 \times 10^{-10} T$, N sec/m^2 (ref. 16).

"The aeronautical and space activities of the United States shall be conducted so as to contribute . . . to the expansion of human knowledge of phenomena in the atmosphere and space. The Administration shall provide for the widest practicable and appropriate dissemination of information concerning its activities and the results thereof."

—NATIONAL AERONAUTICS AND SPACE ACT OF 1958

NASA SCIENTIFIC AND TECHNICAL PUBLICATIONS

TECHNICAL REPORTS: Scientific and technical information considered important, complete, and a lasting contribution to existing knowledge.

TECHNICAL NOTES: Information less broad in scope but nevertheless of importance as a contribution to existing knowledge.

TECHNICAL MEMORANDUMS: Information receiving limited distribution because of preliminary data, security classification, or other reasons.

CONTRACTOR REPORTS: Scientific and technical information generated under a NASA contract or grant and considered an important contribution to existing knowledge.

TECHNICAL TRANSLATIONS: Information published in a foreign language considered to merit NASA distribution in English.

SPECIAL PUBLICATIONS: Information derived from or of value to NASA activities. Publications include conference proceedings, monographs, data compilations, handbooks, sourcebooks, and special bibliographies.

TECHNOLOGY UTILIZATION PUBLICATIONS: Information on technology used by NASA that may be of particular interest in commercial and other non-aerospace applications. Publications include Tech Briefs, Technology Utilization Reports and Technology Surveys.

Details on the availability of these publications may be obtained from:

SCIENTIFIC AND TECHNICAL INFORMATION OFFICE

NATIONAL AERONAUTICS AND SPACE ADMINISTRATION

Washington, D.C. 20546